CHARACTERISTICS OF UPPER HEATED OCEANIC LAYER

FROM SATELLITE OBSERVATIONS

by

AFFONSO DA SILVEIRA MASCARENHAS, JR.

B.S. Universidade de Sao Paulo (Brasil)
(1967)

M.Sc. Instituto de Pesquisas Espacias (Brasil)
(1975)

SUBMITTED IN PARTIAL FULFILLMENT
OF THE REQUIREMENTS FOR THE
DEGREE OF

MASTER OF SCIENCE

at the

MASSACHUSETTS INSTITUTE OF TECHNOLOGY

February, 1979

© Affonso da Silveira Mascarenhas, Jr. 1979

Signature of Author...................
Department of Meteorology, February, 1979

Certified by..
Thesis Supervisor

Accepted by..
Chairman, Departmental Committee on Graduate Students

TABLE OF CONTENTS

CHARACTERISTICS OF UPPER HEATED OCEANIC LAYER

FROM SATELLITE OBSERVATIONS

by

AFFONSO DA SILVEIRA MASCARENHAS, JR.

Submitted to the Department of Meteorology, February, 1979, in partial fulfillment of the requirements for the degree of Master of Science.

ABSTRACT

Velocity of propagation of internal wave packets over the New England American Continental shelf were computed from Landsat A/B images taken in July and August of 1972, 1973, and 1974. A simple two-layer ocean model was used to compute from the velocity of propagation and climatological values of bottom density, the depth of the mixed layer and the amount of heat stored in the upper layer of the ocean. The comparison with in-situ observations showed a good agreement for the amount of heat. Due to the internal wave noise in the hydrographic observations the calculated values for mixed layer depth differ from those computed from satellite data. Charts of distribution of mixed layer depth and amount of heat stored based on 78 observations for the months of July and August are shown. In the Gulf of Maine heat stored values larger for July than August were found. A possible explanation for this anomaly is suggested in terms of air-sea interaction processes.

Thesis Supervisor: Erik Mollo-Christensen
Title: Professor of Oceanography

ACKNOWLEDGEMENTS

1. INTRODUCTION

1.1 The Scope of the Problem

If one chooses not to classify aerial photography as Remote Sensing, the first attempt to extract information about the surface of the oceans sensing remotely came about 25 years ago. The first occasion was when Stommel and Parson (1955), using an Airborne Radiation Thermometer, surveyed the Gulf Stream from an airplane. Broad and synoptic coverage are one of the advantages of this new technique and at the present state of the art we cannot classify Remote Sensing as an independent tool of research, but we have to admit that it is a powerful auxiliary tool.

One hears the argument that only surface observations can be made from airplanes or satellites, while the oceanographers are interested in vertical information as well. This work represents an attempt to correlate information available from satellites and oceanographic platforms as well as trying to infer a three-dimensional picture of oceanic phenomena. One prominent oceanographic feature that plays an important role in the dynamics of the continental shelf waters is the presence of internal wave packets.

As a subsurface feature the internal waves cannot be detected directly by Remote Sensing, but their effects on the surface are visible. Apel and Charnell (1974) explain the internal waves sources and sinks admitting these waves as "daughter" waves generated for a few hours during the peak current velocity by the long-wavelength baroclinic tide occurring at the edges of the continental shelves and island arcs. They then propagate with very low phase speeds, of order 0.25 to 0.5 m/sec, to be absorbed near the bottom where the wave breaks on the shelf.

The association of the distinct surface slicks to internal waves was pointed out by Ewing (1950) and LaFond (1959). There are at least two explanations for why internal wave fields affect the surface of the ocean. The first one suggests that the velocity field of internal waves sweeps together surface oils and materials to form a slick in regions of surface water convergence, increasing the reflectivity of the surface (Ewing, 1950, Shand, 1953). The second explanation is that capillary wave energy is focused in the convergence zones, enhancing the small-scale roughness and decreasing the surface reflectivity (Gargett and Hughes, 1972, Thompson and West, 1972). In either case, quasi-periodic surface features will be produced under light wind conditions, and such effects are very often seen at sea. Under favorable conditions these features can be seen in satellite images as wave packets on the continental shelf areas. The packets are apparently emitted once per tidal period at the shelf edge (Apel et al., 1975). This assumption is supported by the fact that the M_2 component of the internal tide is found to be dominant (Halpern, 1971, Barbee, 1975, Ratray, 1960). Figure 1-1 shows an schematic diagram of the internal wave propagation over the continental shelf and the associated surface slicks.

The eastern coast of the United States (from Cape Hatteras to Nova Scotia) provides favorable conditions for detection of internal wave packets on their continental shelves. The prevalence of internal wave signatures in that area during summer was recognized, and their dependence on the well-defined and relatively shallow thermocline was deduced from their absence during winter months (Apel et al., 1974).

The summer heating thus provides a stratification that can be
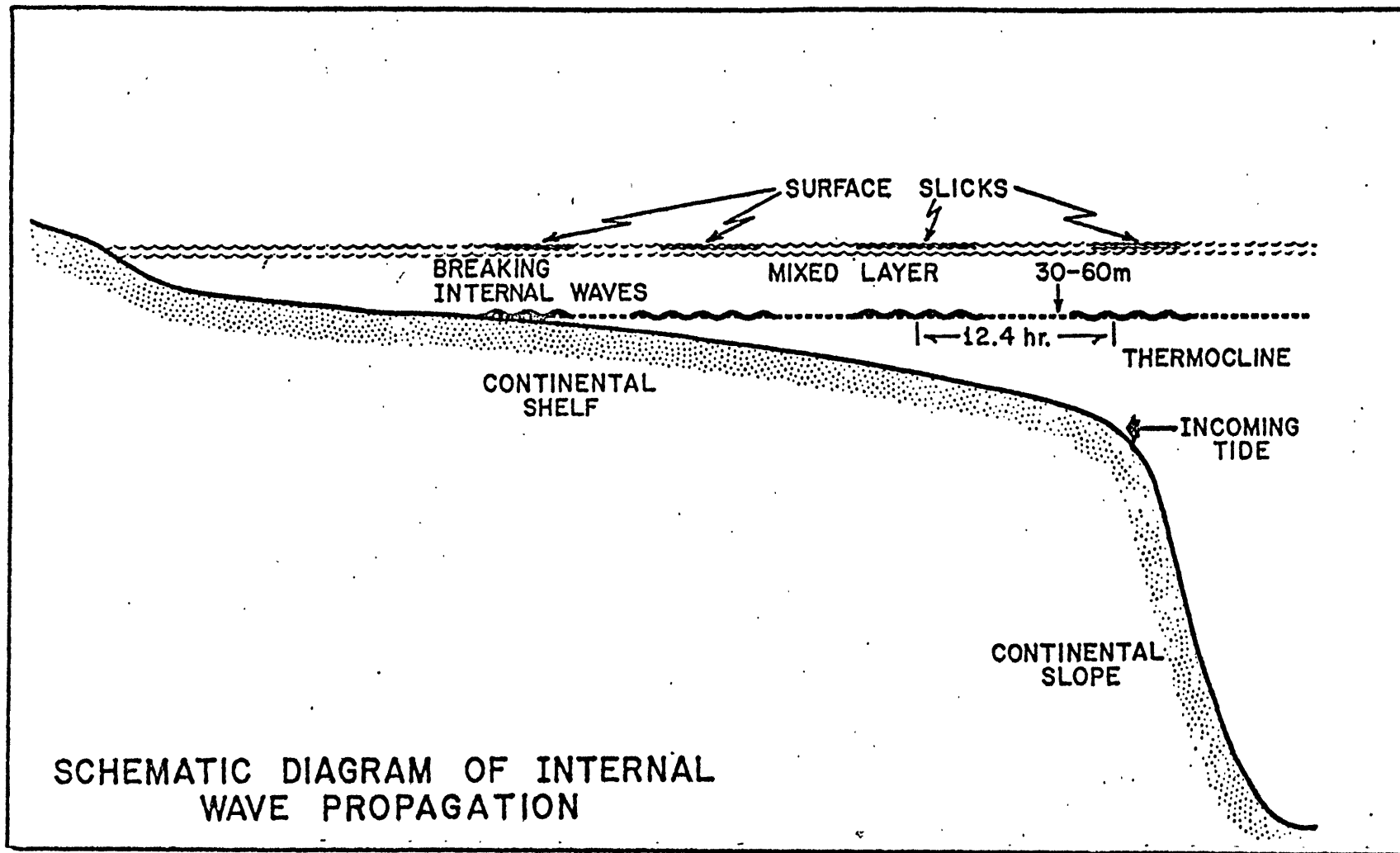
Figure 1.1 - Schematic diagram of the internal wave propagation over the continental shelf (after, Apel 1974).

approximated to an idealized stratification of two homogeneous layers

which have a density difference $\Delta \rho$. This stratification supports

internal gravity waves from which we know the velocity of propagation

taken from the images. This information is enough to compute the depth

of the mixed layer and the heat stored in the seasonal upper warm

layer of the ocean.

The heat stored in the upper ocean affects weather, both climatolo-

gically and synoptically, and the mixing processes in the layer, driven

by wind and thermal effects, also transport oxygen, nutrients and biota.

All these processes show therefore the importance of the knowledge of

the seasonal upper layer.

An extension for a three layer ocean, with the upper and lower

ones homogeneous and the middle layer with a linear variation thermocline

is also made, and the results of the computation are discussed.

1.2 Basic Equations and Assumptions

The basic set of equations is: conservation of momentum, mass, and

equation of state for sea water. The conservation of momentum can be

written (see, for instance, Phillips, 1966)

$$\frac{d\mathbf{v}}{dt} + \boldsymbol{\Omega} \times \mathbf{v} = -\frac{1}{\rho} \nabla p - \nabla \phi \qquad (1.2.1)$$

where $\mathbf{v} = \mathbf{v}(\mathbf{x}, t)$ denotes the velocity of the fluid at prescribed

points in space-time as in an Eulerian description. The velocity compo-

nents following x, y and z are respectively u, v, and w. $\boldsymbol{\Omega}$ is the

rotation vector, or twice the earth's angular velocity. Its magnitude is

$$\Omega = |\underline{\Omega}| = 2\pi/12 \ h^{-1} = 1.45 \times 10^{-4} \ sec^{-1}$$

$\nabla \Phi$, is the gravitational potential, which contains the gravitational term $\underline{g} = (0, 0, -g)$ representing the apparent gravitational acceleration, or the true (central) gravitational acceleration modified by the small (centrifugal) contribution normal to the axis of the earth's rotation. The term ∇p represents the pressure gradient forces, and ρ is the density of sea water given as

$$\rho = \rho \ (T, S, P) \tag{1.2.2}$$

The conservation of mass is expressed by

$$\frac{\partial \rho}{\partial t} + \nabla \cdot (\rho \underline{v}) = 0 \tag{1.2.3}$$

As in the Eulerian formulation, the total time derivative (derivative following the motion) is the sum of the time rate of change at a fixed point and a convective rate of change

$$\frac{d}{dt} = \frac{\partial}{\partial t} + (\underline{v} \cdot \nabla)$$

1.2.1 The Boussinesq Approximation

If we assume a basic state being steady and at rest (1.2.1) reduces to

$$\frac{\partial P_B}{\partial z} + \rho_B g = 0 \qquad (1.2.1.1)$$

and if we subtract this equation from (1.2.1) we get

$$\rho \frac{dv}{dt} + \rho \mathcal{R} \times v + \nabla \tilde{p} + (\rho - \rho_B) g = 0 \qquad (1.2.1.2)$$

where $\tilde{p} = p - P_B$

In the ocean the difference between the actual state and the reference state is the result primarily of surface heating or cooling, whose influence is distributed by the process of convection and mixing. Surface water in regions of low salinity and high temperature has a density as low as 1.02 gm/cm^3. Water in the deepest trenches is subjected to the highest pressures and has a density as high as 1.07 gm/cm^3. So the maximum range is only about 5%!

Boussinesq in 1877 introduced an important approximation, namely; "The variations in the fluid density are neglected in so far as they influence the inertia terms, variations in the weight (or buoyancy) of the fluid may not be negligible."

So in (1.2.1.2) it is possible to approximate ρ by ρ_B. But taking into account the fact that in the ocean the scale of vertical movements is much less than the scale height, an even greater simplifi-

cation can be done, also since the reference density ρ_s varies

little from the constant mean value ρ_o . So we can rewrite (1.2.1.2)

$$\frac{d\mathbb{V}}{dt} + \mathfrak{R}\times\mathbb{V} + \frac{\nabla}{\rho_0}(p-p_B) + \frac{(\rho-\rho_B)}{\rho_0}g\mathbb{J} = 0 \qquad (1.2.1.3)$$

Using the fact that the mean value ρ_o is hydrostatic, we can modify

the buoyancy and pressure terms in (1.2.1.3) to get finally

$$\frac{d\mathbb{V}}{dt} + \mathfrak{R}\times\mathbb{V} = -\frac{1}{\rho}\nabla p - g\mathbb{J}\frac{(\rho-\rho_o)}{\rho_0} \qquad (1.2.1.4)$$

where p now represents the difference between the actual and the

hydrostatic pressure in an ocean at rest with constant density ρ_o .

Let us see now the effect of Boussinesq approximation in the conser-

vation of mass equation (1.2.3). If $\rho = \rho_o$ we will not have strati-

fication at all. Since we want Boussinesq approximation as well as

stratification, we say that our density is not constant, but varies a

little around the mean value ρ_o . This statement can be written

analytically as

$$\rho = \rho_o + \bar{\rho}(z) + \rho' \qquad (1.2.1.5)$$

where $\bar{\rho}(z)$ is the added stratification and ρ' is the variation

in the density field due to internal waves. The expression (1.2.1.5)

is called quasi-Boussinesq approximation. The new conservation of mass equation is

$$\frac{d\rho'}{dt} + \omega \frac{\partial \bar{\rho}}{\partial z} = 0 \qquad (1.2.1.6)$$

The conditions for validity of Boussinesq approximation are:

a) The actual density distribution differs only slightly from the reference state;

b) The vertical scale of motion is small compared with the scale height; $\mathcal{H} \sim O(200 \text{ km}) \gg H \sim O(4 \text{ km})$

c) The Mach number of the flow is very small; for water at 15°C, c = 1470 m/sec, u = 5 cm/sec, M = 0.34×10^{-4},

so for the ocean all the requirements are fulfilled.

Expanding (1.2.2) about the basic state density ρ_B and neglecting the second order terms we get

$$\rho' = \bar{\rho} \left(-\alpha T' + k P' + \gamma S' \right) \qquad (1.2.1.7)$$

where

$$\alpha = -\frac{1}{\rho} \left(\frac{\partial \rho}{\partial T} \right)_{P,S} \qquad \text{(coefficient of thermal expansion)} \quad ;$$

$$k = \frac{1}{\rho} \left(\frac{\partial \rho}{\partial P} \right)_{T,S} \qquad \text{(coefficient of isothermal compressibility)};$$

$$\gamma = \frac{1}{\rho} \left(\frac{\partial \rho}{\partial S} \right)_{P,T} \qquad \text{(fractional increase in density per unit increase in salinity keeping T and P constant)}$$

If we substitute (1.2.1.7) in the right-hand side of (1.2.1.4), the vertical component of (1.2.1.4) has on the right-hand side the terms

$$-\frac{1}{\bar{\rho}} \frac{\partial p'}{\partial z} + g\alpha T' - gkp' - g\gamma S'$$

For oceanic motions the vertical scale of variation H is of order 10^5 cm, so that the first term has magnitude $|p'|/H$. The isothermal compressibility k has a magnitude of 4.5×10^{-11} in cgs units, so that the term gkp' has a magnitude $|p'|/Hs$, where Hs = 1/gk is the scale height for sea water. Its value is 2×10^7 cm, i.e. substantially larger than the vertical scale H. So the pressure fluctuation term in the equation of state is dynamically insignificant (Veronis, 1973). To be fair we need to compare the other terms; in the second one, (52 $\leqslant \alpha \leqslant$ 335) x 10^{-6} for S = 35 ‰ , so will be of order $|T'|$ x 10^{-5}, and the last one is also of the order of $|S'|$ x 10^{-5}, so we can approximate the equation of state to

$$\rho = \bar{\rho}(1 - \alpha T' + \gamma S')$$

(1.2.1.8)

Phillips (1966) showed that, since the entropy of a given fluid element varies only as a result of molecular diffusion and (very near the free surface) of radiative transfer,

$$\nabla \cdot V = \frac{g\omega}{c^2}$$

and also that the ratio between the left hand and right hand side of the above expression is or order Z/H, negligibly small and so

$$\nabla \cdot V = O$$

(1.2.1.9)

is a good approximation for internal waves.

1.2.2 The Brunt-Väisälä frequency

At a fixed oceanographic station in the sea, continuous measurements of temperature, or any other physical or chemical property of sea water, shows variations of these properties at a fixed depth. This variability is frequently found particularly near the highly stratified thermocline. Quoting Turner (1973):

> A body of homogeneous, inviscid incompressible fluid at rest is in a state of neutral equilibrium. At every point the weight of a fluid element is then exactly balanced by the pressure exerted on it by neighboring fluid, and this continues to hold true if the elements are displaced to another position of rest. When ρ varies the hydrostatic equation
>
> $$p = p_0 - g \int_0^z \rho \, dz$$
>
> (1.2.2.1)
>
> shows that the fluid (in the absence of diffusion) is in equilibrium only when the density as well as the pressure is constant in every horizontal plane. This equilibrium stratification is stable when the heavier fluid lies below, since tilding of a density surface will produce a restoring force. The resulting motion can overshoot the equilibrium position and oscillate about it, thus giving rise to internal waves.

To find an analytic expression for this natural frequency of oscil-
lation that stems from differences in density we take the z component
of the momentum equation for an inviscid stratified fluid

$$\frac{d\omega}{dt} = -\frac{1}{\bar{\rho_0}}\frac{\partial P}{\partial z} - g\frac{(\bar{\rho}-\bar{\rho_0})}{\bar{\rho_0}} = \frac{d^2\varsigma}{dt^2} \tag{1.2.2.2}$$

where ς is the vertical displacement of a fluid element from its
position of equilibrium. Using the relation

$$\bar{\rho} - \bar{\rho_0} = -\varsigma\frac{d\bar{\rho}}{dz}$$

and assuming no pressure variation during the displacement, we get the
ordinary differential equation

$$\frac{d^2\varsigma}{dt^2} + \left(\frac{g}{\bar{\rho_0}}\frac{\partial\bar{\rho}}{\partial z}\right)\varsigma = 0$$

which has as solution an oscillation with frequency N, where

$$N^2 = -\frac{g}{\bar{\rho}}\frac{\partial\bar{\rho}}{\partial z} \tag{1.2.2.3}$$

N is called Brunt-Väisälä frequency or stability frequency, and is the
frequency at which a fluid element at rest will oscillate if displaced

from its equilibrium condition.

If in the equation (1.2.2.2) we had introduced the Boussinesq approxi-mation, i.e. ρ_0 , the hydrostatic relation would have ρ instead of $\bar{\rho}$, and also $\rho - \rho_0 = -\zeta \frac{d\bar{\rho}}{dz}$. These changes would give us a different Brunt-Väisälä frequency, namely,

$$N^2 = -\frac{g}{\rho_0} \frac{\partial \bar{\rho}}{\partial z} \qquad (1.2.2.4)$$

The former one is better when applied to exponential extratification, because it will give a constant N; meanwhile the last one is good for linear stratification, for the same reason. Typical values of N are

at pycnocline ~ 2 cycles per hour

at abyssal water $\sim$ .5 cycles per hour

When we are dealing with deep water an extra term arises in the definition to take into account the compressibility. For shallow water we just need to use $\rho_{S,T,0}$ values, i.e. density at described values of temperature and salinity and at zero pressure (assumed to be the surface). So we can compute σ_t from T and S and find ρ from the relation

$$\sigma_t = (\rho_{S,T,0} - 1) \cdot 10^3 \qquad (1.2.2.5)$$

1.2.3 The Equation for Internal Waves

The basic set of equations the comprises the so-called Boussinesq approximation are equations (1.2.1.4), (1.2.1.6) amd (1.2.1.9), given

below in component form

$$\frac{\partial u}{\partial t} + \frac{1}{\rho_o} \frac{\partial P}{\partial x} - f\upsilon = - (\mathbf{v} \cdot \nabla) u \qquad (1.2.3.1)$$

$$\frac{\partial \upsilon}{\partial t} + \frac{1}{\rho_o} \frac{\partial P}{\partial y} + fu = - (\mathbf{v} \cdot \nabla) \upsilon \qquad (1.2.3.2)$$

$$\frac{\partial w}{\partial t} + \frac{1}{\rho_o} \frac{\partial P}{\partial z} - \frac{(\rho - \rho_o)}{\rho_o} g = - (\mathbf{v} \cdot \nabla) w \qquad (1.2.3.3)$$

$$\frac{\partial u}{\partial x} + \frac{\partial \upsilon}{\partial y} + \frac{\partial w}{\partial z} = 0 \qquad (1.2.3.4)$$

$$\frac{\partial \rho'}{\partial t} + w \frac{\partial \bar{\rho}}{\partial z} = - (\mathbf{v} \cdot \nabla) \rho' \qquad (1.2.3.5)$$

where

$$\rho = \rho_o + \bar{\rho}(z) + \rho'(x, y, z, t) \qquad (1.2.3.6)$$

After some manipulation with the above equations we get the equation

$$\frac{\partial^2}{\partial t^2} (\nabla^2 w) + f^2 \frac{\partial^2 w}{\partial z^2} + N^2 \nabla_2^2 w = \mathcal{N} \qquad (1.2.3.7)$$

where $\mathcal{N}$ stands for the non linear terms and

$$\nabla_2^2 = \frac{\partial^2}{\partial x^2} + \frac{\partial^2}{\partial y^2}$$

Equation (1.2.3.7) is the equation of the internal waves in an ocean with arbitrary Brunt-Väisälä distribution N(z). For infinitesimal

disturbances in the absence of a mean shear, the right hand side of (1.2.3.7) is negligible and the governing equation is linear

$$\frac{\partial^2}{\partial t^2}(\nabla^2 \omega) + f^2 \frac{\partial^2 \omega}{\partial z^2} + N^2 \nabla_2^2 \omega = 0 \ . \tag{1.2.3.8}$$

If we have stated instead of (1.2.3.6) the following;

$$\rho = \bar{\rho}(z) + \rho' \ ,$$

we would get an extra term in equation (1.2.3.7), namely,

$$- \frac{N^2}{g}(\omega_{tt} + f^2 \omega)_z \ .$$

For a time harmonic variation like

$$\omega = W(z) \exp\left[i(\mathbb{k}_0 \mathcal{X} - \sigma t)\right] \ , \tag{1.2.3.9}$$

where $\mathbb{k} = \{k, \ell\}$ is the horizontal wave number and $\mathcal{X} = \{x, y\}$ is the horizontal coordinate

The substitution of (1.2.3.9) in (1.2.3.8) gives the equation for the vertical movements of the field

$$\frac{d^2 W}{dz^2} + \frac{(\sigma^2 - N^2)}{(f^2 - \sigma^2)} \alpha^2 W = 0 \quad , \tag{1.2.3.10}$$

where $\qquad \alpha^2 = k^2 + \ell^2 .$

The boundary condition at the bottom is

$$W = u \frac{\partial h}{\partial x} + v \frac{\partial h}{\partial y} \quad , \quad \text{at} \quad z = -h(x,y) \tag{1.2.3.11}$$

or for a flat bottom

$$w = 0 \quad , \quad \text{at} \quad z = -h . \tag{1.2.3.12}$$

In the surface neglecting the atmospheric pressure input to internal waves, and non linear terms we have

$$\frac{\partial^2}{\partial t^2}\left(\frac{\partial w}{\partial z}\right) + f^2 \frac{\partial w}{\partial z} + g \nabla_z^2 w = 0 \quad , \quad \text{at} \quad z = 0 \tag{1.2.3.13}$$

correct only to the first order. The internal waves in the ocean produce only very small vertical displacements of the free surface, so the free surface boundary condition can be taken as

$$W = 0 \quad , \text{ at } \quad z \simeq \eta = 0 .$$

(1.2.3.14)

Since the condition,

$$\frac{\sigma_i^2 - f^2}{g \alpha_s} \left(\frac{N_{(0)}^2 - \sigma_i^2}{\sigma_i^2 - f^2} \right) \ll 1$$

(1.2.3.15)

is usually satisfied strongly. Here σ_i stands for internal wave frequency, α_s for surface wave number and $N_{(0)}^2$ for Brunt-Vaisala frequency very near the surface.

2. THE MODELS, THEIR SOLUTION AND APPLICATIONS.

2.1 The Two Layer Model

Frequently the ocean can be approximated by a two layer model. This

occurs either when the upper layer of the ocean has been well-mixed

as a result of a storm or by the action of the trade winds or when it

is heated during the summer months. In each case the thermocline is

fairly abrupt and separates water masses above and below, each of which

is almost homogeneous (see Fig. 2.1).

Let there be two layers of inviscid, incompressible homogeneous

fluid, the lower one with density ρ_2 and the upper one with density

ρ_1 , the bottom being described by the function b(x,y). The h's

are the equilibrium thickness of each layer and the ζ 's are the devia-

tion of the surfaces from its equilibrium position. The equation for

the upper layer will be

$$\frac{du_1}{dt} - f\bar{v}_1 = -g\frac{\partial \zeta_1}{\partial x} \quad , \tag{2.1.1}$$

$$\frac{dv_1}{dt} + fu_1 = -g\frac{\partial \zeta_1}{\partial y} \quad , \tag{2.1.2}$$

$$\frac{\partial}{\partial t}(\zeta_1 - \zeta_2) + \frac{\partial}{\partial x}(u_1 h_1) + \frac{\partial}{\partial y}(v_1 h_1) = 0 \tag{2.1.3}$$
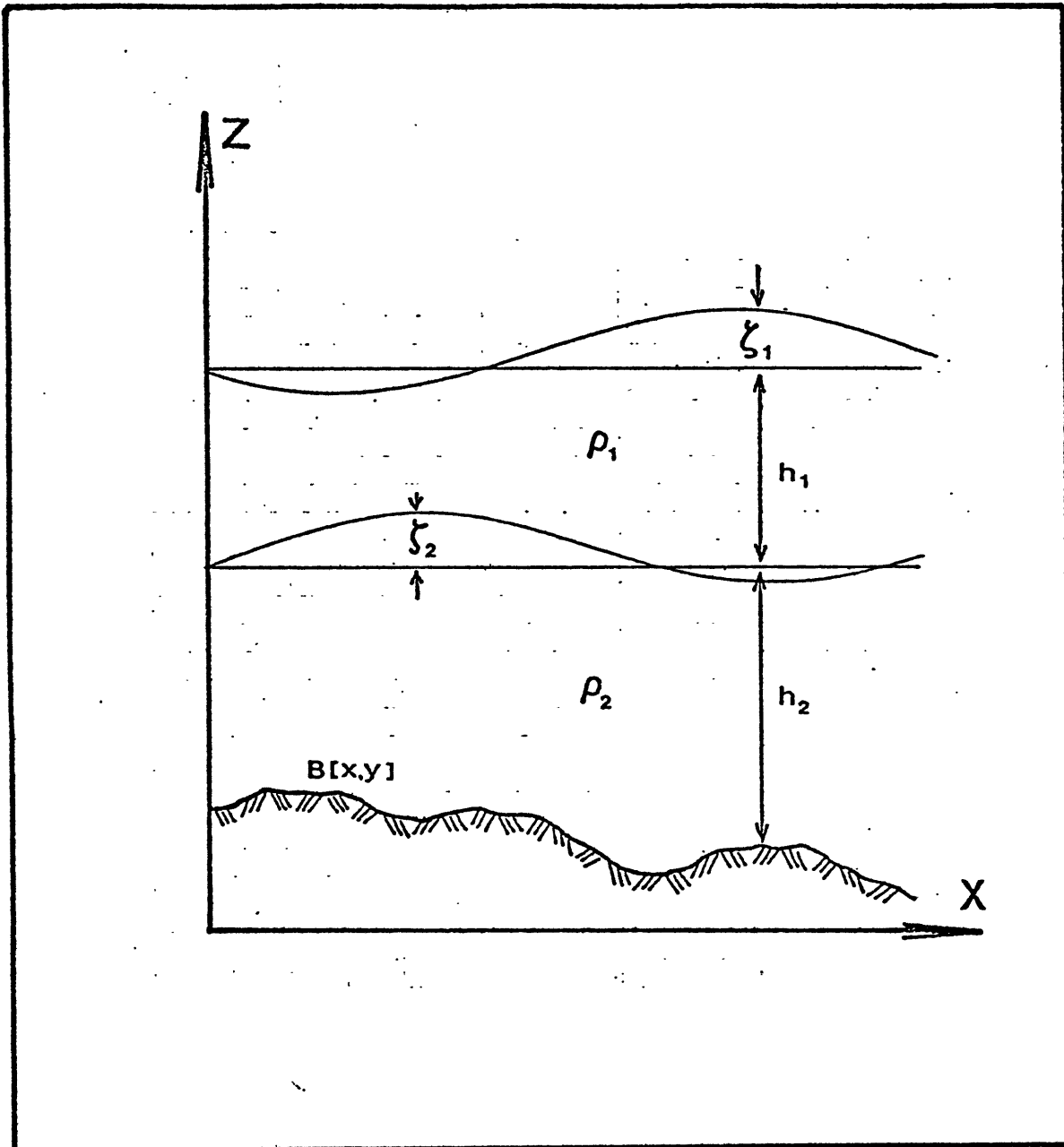
and for the lower layer

Figure 2.1 - The two-layer model schematically.

$$\frac{du_2}{dt} - f v_2 = -g \frac{\rho_1}{\rho_2} \frac{\partial \zeta_1}{\partial x} - g \frac{(\rho_2 - \rho_1)}{\rho_2} \frac{\partial \zeta_2}{\partial x} \ , \tag{2.1.4}$$

$$\frac{dv_2}{dt} + f u_2 = -g \frac{\rho_1}{\rho_2} \frac{\partial \zeta_1}{\partial y} - g \frac{(\rho_2 - \rho_1)}{\rho_2} \frac{\partial \zeta_2}{\partial y} \ , \tag{2.1.5}$$

$$\frac{\partial \zeta_2}{\partial t} + \frac{\partial}{\partial x}(u_2 h_2) + \frac{\partial}{\partial y}(v_2 h_2) = 0 \ . \tag{2.1.6}$$

This kind of problem was first investigated by Stokes (1847),

(see for instance, Lamb, 1932, article 231). He solved for a wave

propagating along the x axis with the upper surface of the upper fluid

free. For the special case where the depth of the lower fluid is great

compared with the wavelength and the upper layer depth is much less than

the wavelength he found

$$\bar{c}^2 = \frac{\sigma^2}{k^2} = h_1 g \frac{\Delta \rho}{\rho_2} \ . \tag{2.1.7}$$

The same solution was worked out in a very elegant fashion by Phillips

(1966), solving the internal wave equation (1.2.3.10) with f=0 and

using a delta function for the Brunt-Väisälä function.

In view of the application of (2.1.7) to internal waves with semi-

diurnal period over the continental shelf let us see the implication of

the assumptions on this practical application. The continental shelf in

the region between Nova Scotia and Cape Hateras has a mean depth of 100 m.

Very few internal waves were detected over the continental slope where

$200 \lesssim H \lesssim 1000$ meters. The measurements of the distance between the internal wave packets showed that the wavelengths of the waves vary from 400 to 2200 m. This means, assuming $h_2 = 7\times10^3$ cm, $1.01 \geq kh_2 \geq 0.2$ or that $5.07 \geq \coth kh_2 \geq 1.25$! So the assumption that $\coth kh_2 = 1$ is only approximately true for waves with smaller wavelengths, and if applied to larger wavelengths will give errors.

The other assumption was that the upper layer is much less than the wavelength or $kh_1 \ll 1$, for $h_1 = 3\times10^3$ cm. We have $8.57\times10^{-2} \lesssim kh_1 \lesssim 4.71\times10^{-1}$, that can be considered a fair approximation. Now remains the question, can we neglect the Coriolis parameter f in the equations? What would be the consequences if we take it into account?

If we write down equation (1.2.3.10) again

$$\frac{d^2W}{dz^2} + \frac{(\sigma^2 - N^2)}{(f^2 - \sigma^2)}\alpha^2 W = 0 \qquad (2.1.8)$$

and the patching conditions,

$$W(-d + \varepsilon/2) = W(-d - \varepsilon/2) \qquad (2.1.9)$$

and

$$\left.\frac{dW}{dz}\right|_{-d+\varepsilon/2} - \left.\frac{dW}{dz}\right|_{-d-\varepsilon/2} = \frac{\alpha^2 W_{-d}}{\sigma^2 - f^2}\left[\sigma^2 \varepsilon - g\frac{(\rho_2 - \rho_1)}{\rho_0}\right] , \qquad (2.1.10)$$

where $d \pm \epsilon$ is the depth of the discontinuity in density, so $N(z)$ is zero outside this region. The solution of equation (2.1.8) and the conditions (2.1.9) and (2.1.10) lead to the dispersion relation:

$$\sigma^2 = f^2 + \frac{\alpha^2 g (\rho_2 - \rho_1)}{\mu \rho_0} \left[\coth \mu d + \coth \mu (H-d) \right]^{-1} , \qquad (2.1.11)$$

where $\mu^2 = \sigma^2 \alpha^2 / \sigma^2 - f^2$ and H is the depth of the flat bottom. In this section, and when needed, we are going to choose our coordinates system such that our horizontal wave number $a = k$, can be thought of as in the x direction.

Since one of our aims is to compute the depth of the mixed layer we need to work out the expression (2.1.11). The other aim is to compute the amount of heat stored in the upper layer and as we shall see later on, only the velocity of propagation c is enough.

Under the assumption

$$\coth \mu H \sim O(1) \qquad \text{, consequently}$$

$$\coth \mu d + \coth \mu (H-d) \sim \coth \mu d + 1 .$$

We can rewrite (2.1.11) as

$$(\sigma^2 - f^2)^{1/2} = \frac{g'}{c} (1 + \coth \mu d)^{-1} ,$$

and the expression for the mixed layer depth will be

$$d = \frac{(c^2 - f^2/\alpha^2)^{1/2}}{\alpha c} \coth^{-1} \left[\frac{g'}{\alpha c} \frac{1}{(c^2 - f^2/\alpha^2)^{1/2}} \right] . \qquad (2.1.12)$$

The above assumption will give higher errors for shallow waters,
i.e. $h < 60$ m.

It is clear that if we make $f=0$ and $\alpha d \ll 1$ the expression
(2.1.12) will reduce to (2.1.7). In Chapter 6 the results of computation
of d using (2.1.12) and (2.1.7) will be discussed, but we can anticipate
that the inclusion of f does not change the results at all, of course
for practical purposes.

2.2 The Three-Layer Models

A more realistic model is a three-layer model with a density profile and a Brunt-Vaisala frequency as shown in Figure 2.2. In the model the upper layer has a constant density ρ_1, the bottom layer has a constant density ρ_3, and in the middle we have a linearly varying density profile like

$$\rho_2(z) = \rho_1 + a(z + h_1) \qquad , \qquad (h_1 \geq z \geq h_1 + h_2) \qquad (2.2.1)$$

where

$$a = \frac{\Delta\rho}{\Delta z} = \frac{\rho_3 - \rho_1}{-h_2} \quad .$$

The Brunt-Vaisala frequency in this layer is

$$N^2 = -\frac{g}{\bar{\rho}}\frac{\partial\rho}{\partial z} = \frac{2g}{h_2}\left(\frac{\rho_3 - \rho_1}{\rho_3 + \rho_1}\right) = \frac{g'}{h_2} \qquad , \qquad (2.2.2)$$

where g' = $g\Delta\rho/\bar{\rho}$ is the reduced gravity for a two layer ρ_1 and ρ_3, and where we have used a mean value $(\rho_1 + \rho_3)/2$. Recalling the equation for vertical motions of internal waves (1.2.3.10)

$$\frac{d^2 W}{dz^2} + \left(\frac{\sigma^2 - N^2}{f^2 - \sigma^2}\right)\alpha^2 W = 0 \qquad , \qquad (2.2.3)$$
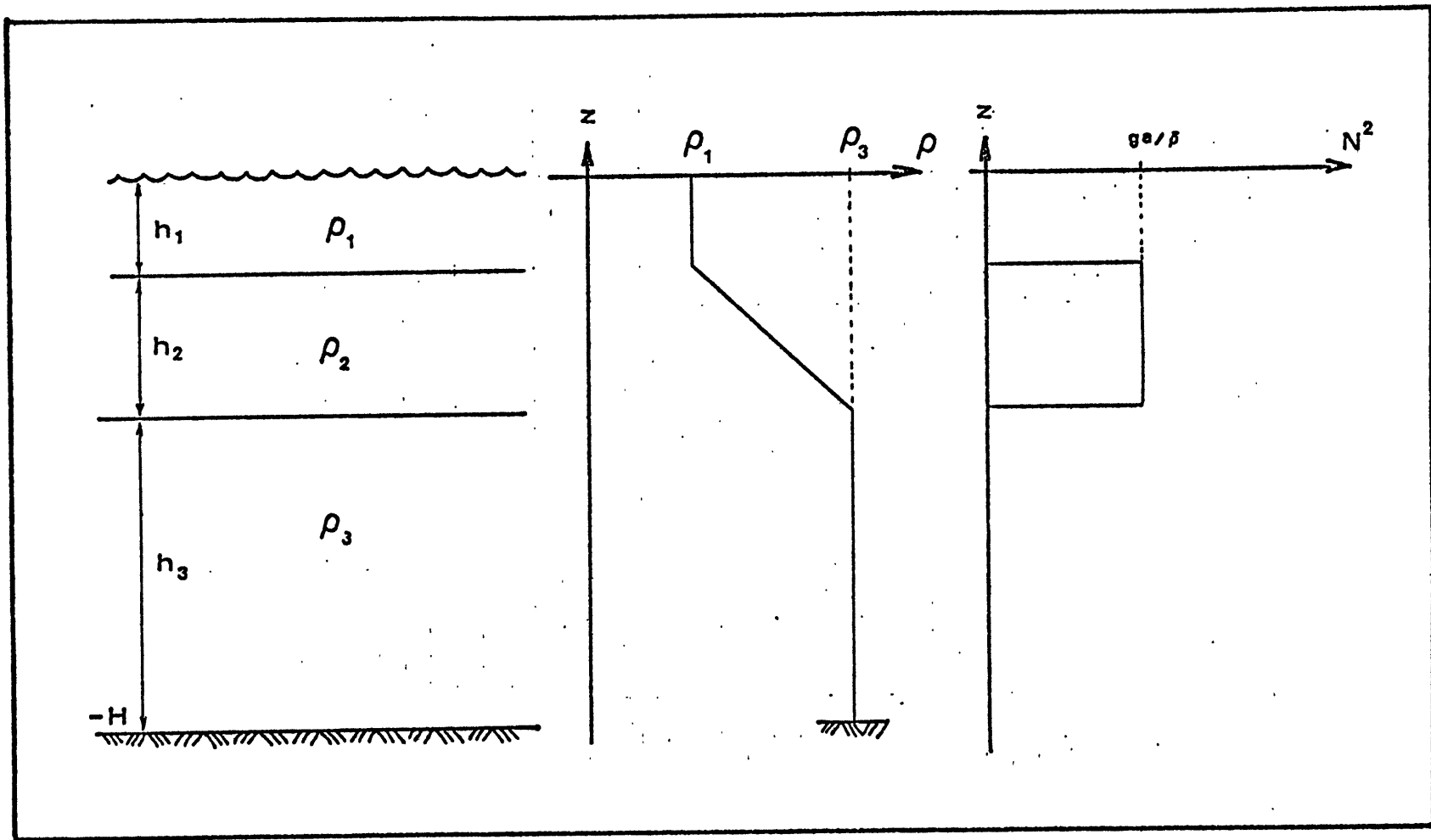
Figure 2.2 - The three-layer model, density distribution and Brunt-Vaisala frequency.

with the boundary conditions

$$W = 0 \qquad , \quad at \qquad z = 0, -H . \qquad (2.2.4)$$

The solutions of (2.2.3) and (2.2.4) are:

$$W_1 = B_1 \sinh \mu z \qquad , \quad -h_1 \leq z \leq 0 \quad , \qquad (2.2.5)$$

$$W_2 = A_2 \cos \delta z + B_2 \sin \delta z \quad , \quad -h_2 - h_1 < z < -h_1 \quad , \qquad (2.2.6)$$

$$W_3 = B_3 \sinh \mu (z + H) \qquad , \qquad -H \leq z \leq -h_1 - h_2 \quad , \qquad (2.2.7)$$

where the indices 1, 2 and 3 hold for the upper, middle and bottom layers and

$$\delta^2 = \left(\frac{N^2 - \sigma^2}{\sigma^2 - f^2} \right) \alpha^2 \qquad and \qquad \mu^2 = \frac{\alpha^2 \sigma^2}{\sigma^2 - f^2} \quad . \qquad (2.2.8)$$

To solve the problem completely we need four more conditions, that is, the conditions in the interface between the layers. The first one is that w must be continuous across the interface, i.e.,

$$[W] = 0 \qquad , \quad at \qquad z = -h_1 \quad , \quad -h_1 - h_2 \quad . \qquad (2.2.9)$$

The second one is obtained by integration of (2.2.3) across the

interfaces,

$$\left[\frac{dw}{dz}\right] = 0 \qquad , \quad at \qquad z = -h_1 \; , \; -h_1 - h_2 \; . \qquad (2.2.10)$$

The application of these conditions to the solutions (2.2.5-7) gives

rise to a set of homogeneous equations that admit a solution different

from the trivial one, only if

$$\begin{vmatrix} \sinh \mu h_1 & \cos \delta h_1 & -\sin \delta h_1 & 0 \\ 0 & \cos \delta(h_1+h_2) & \sin \delta(h_1+h_2) & -\sinh \mu h_3 \\ \frac{\mu}{\delta}\cosh \mu h_1 & -\sin \delta h_1 & -\cos \delta h_1 & 0 \\ 0 & -\sin \delta(h_1+h_2) & \cos \delta(h_1+h_2) & -\frac{\mu}{\delta}\cosh \mu h_3 \end{vmatrix} = 0 \quad ,$$

where $h_3 = H-h_1-h_2$. The above determinant is the dispersion relation

of the wave, namely

$$\left(\frac{\mu}{\delta}\right)^2 + \cot \delta h_2 \left(\tanh \mu h_1 + \tanh \mu h_3\right)\frac{\mu}{\delta} - \tanh \mu h_1 \tanh \mu h_3 = 0 \qquad (2.2.11)$$

where from (2.2.8)

$$\frac{\mu}{\delta} = \frac{\sigma^2}{N^2 - \sigma^2} \qquad (2.2.12)$$

If we neglect the Coriolis parameter f the dispersion relation

(2.2.11) can be rewritten as

$$\gamma^2 - \tanh \alpha h_1 \tanh \alpha h_3 + \gamma \cot \delta h_2 \left(\tanh \alpha h_1 + \tanh \alpha h_3 \right) = 0 \qquad (2.2.13)$$

where now $\delta^2 = \dfrac{(N^2 - \sigma^2) \alpha^2}{\sigma^2}$, $\gamma = \dfrac{\mu}{\delta}$ and α is the wave number here considered only in the x direction for the sake of simplicity.

According to Roberts (1975), care must be taken in making the Boussinesq approximation when this model of density distribution is used, particularly when a finite depth is assumed (Benjamin, 1967). It seems that the Boussinesq approximation is not valid for waves which are sufficiently long compared to the thermocline thickness h_2 (Thorpe, 1968). Here we have solved separately for each layer so it is still valid to approximate

$$\tanh \alpha h_1 \sim \alpha h_1$$
$$\tanh \alpha h_3 \sim \alpha h_3$$

since $\alpha h_1, \alpha h_3 \ll 1$. But we cannot approximate the $\cot \delta h_2$ in (2.2.11), so

$$\gamma^2 - \alpha^2 h_1 h_3 + \gamma \alpha \left(h_1 + h_3 \right) \cot \delta h_2 = 0 \qquad (2.2.14)$$

factor the above dispersion relation and expanding small terms

$$\gamma^2 = \alpha^2 h_1 h_3 \left[1 - \frac{\alpha \left(h_1 + h_3 \right)}{\gamma} \cot \delta h_2 \right] \qquad (2.2.15)$$

so to the first order,

$$c^2 = (N^2 - \sigma^2) h_1 h_3 \qquad \qquad (2.2.16)$$

We see that even a first approximation of the dispersion relation for the three-layer model is useless for our purposes because it introduces variables that we cannot measure.

The first approximation for the group velocity will be

$$C_G = c (1 - \alpha^2 h_1 h_3) \qquad \qquad (2.2.15)$$

where c is the phase velocity (2.2.16).

3. DATA AND MEASUREMENTS

3.1 What the Internal Gravity Waves on the Continental Shelf Look Like

Surface manifestations of oceanic internal waves have been observed by many investigators, and their dependence upon wave-associated surface currents has been recognized for at least a generation (Ewing, 1950). The surface signatures are most evident on a relatively calm sea and take the form of a quasi-periodic, long-length modulation of the capillary-ultragravity wave spectrum; the scale of the modulation is usually of the order of hundreds of meters (Gargett and Hughes, 1972). Visible manifestations on the ocean surface are theorized as being due to at least two mechanisms, either of which modulates the short surface wave structure rather than a change in optical reflectivity or absorptivity at depth. The first theory suggests that the high velocity of surface waves arising from the large internal wave amplitude sweeps together surface oils and debris to form a slick in regions of surface water convergence, thus increasing the specular reflection and decreasing the diffuse scattering over the convergence region.

On the other hand, Gargett and Hughes (1972) have suggested another mechanism based on the observation that surface waves seem to change their direction of propagation over the crests of internal waves. They therefore investigated the interaction between surface waves and a periodic mean current induced by an internal wave. They found that if $c_{g_s}(\cos \Phi) > c_{p_i}$ over an internal wave crest, (c_{g_s} - surface wave group speed, c_{p_i} - internal wave phase speed, Φ - angle between c_{g_s} and c_{p_i}) i.e., if the surface wave groups overtake the internal wave,

then the surface waves will tend to propagate in the direction of the
internal wave and their amplitudes will increase. If $c_{g_s}(\cos \Phi) < c_{p_i}$
over an internal wave crest, i.e., if the surface wave groups are over-
taken by the internal wave, the direction of the surface waves is turned
away and their amplitudes decrease. Over troughs, the opposite effects
occur. So for a given internal wave field, the system will have singu-
larities for certain surface waves. Therefore, there will be regions
where none of these surface waves can exist, and these regions will
appear as surface slicks.

Periodic features observed in the United States eastern coast in
certain ERTS A/B images have been identified as surface slicks, so
associated with internal waves. These features are only present during
northern hemisphere summer months. This suggests that these internal
waves are present when summer solar heating stratifies the water suf-
ficiently well to support such oscillations. When fall and winter wind
action mixes the shelf water down to the bottom, the waves no longer
appear. Figure 3.1a and 3.1b show enlargements of ERTS images where
internal wave manifestations can be seen.

The common properties of these waves as they appear in these figures
can be summarized as follows (Apel et al., 1974, 1975, 1976).

a) The waves occur in groups or packets of width L = 3 to 5 km,
usually landward of the continental slope and separated by distances D,
which range from 4 to 40 km;

b) the crests are nearly always oriented parallel to the local
bottom topography or can be loosely associated with some topographic
feature seaward of their observed position, or both;
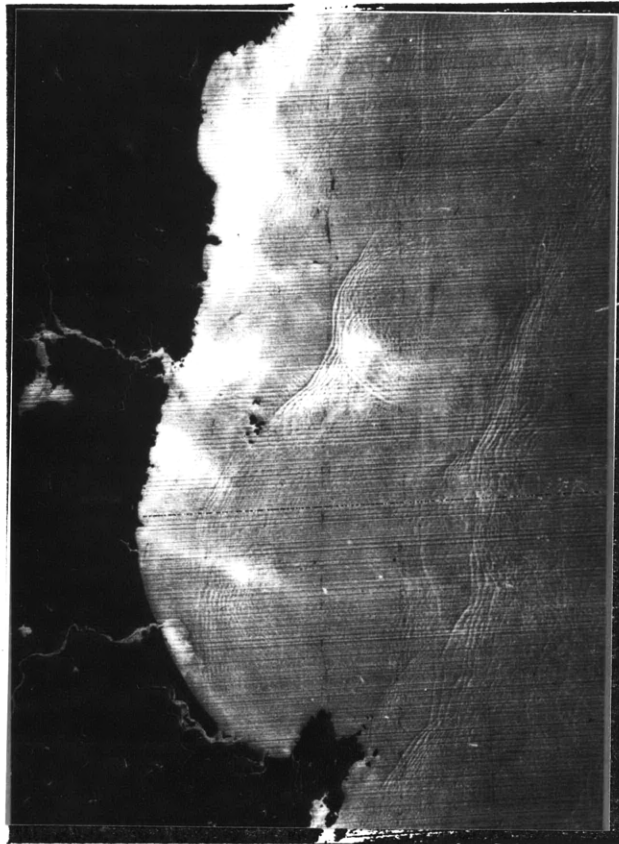
Figure 3.1a - Enlargement of Landsat image 1364-14550 taken on 23 july 1973.We can see two wave packets north of Cape Ann; the waves propagate shoreward.
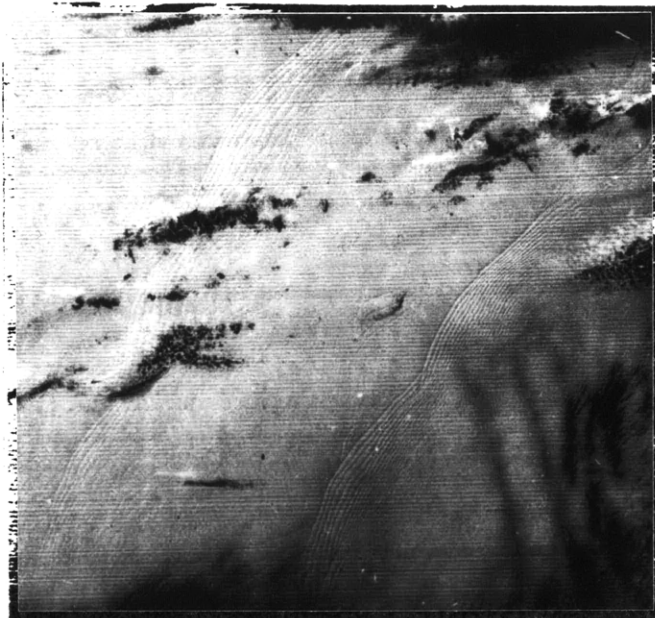

Figure 3.1b - Enlargement of Landsat image 1365-15013 taken on 23 july 1973.We can see two wave packets propagating towards the upper left corner of the image.The geographical location is south of Long Island.

c) the wavelengths fall between 400 and 2200 m, depending on the geographical area; within a given packet there often is a monotonic decrease in wavelength, varying from λ_o at the front to $\lambda < \lambda_o$ at the back of the group;

d) the lengths of the crests, M, fall between 5 to 100 km, with a decrease in crest length occurring from front to back of the group;

e) the widths of the slicks, ls, are often small compared to the lead wavelength λ_o ;

f) the crests are curved in a horizontal plane with their convex sides pointed in the direction of propagation; the radii of curvature Rc, range from essentially infinity to a few kilometers;

g) as the packet progresses up on the shelf, there is some evidence of a continued increase in the wavelengths throughout; this may be accounted for by a combination of linear dispersion and nonlinear effects akin to solitary wave behavior.

All the parameters of the internal wave packets are shown in a schematic way in Fig. 3.2.

Although there is no doubt about the identification of the above discussed features as internal waves, some non-users of satellite data can argue about the identification of the same. Here are some justifications (Apel and Charnel, 1976):

i) They exhibit the correct properties and behavior of internal waves.

ii) If they were surface waves, the average wavelength of 1000 m would imply a swell with the extremely long period of 24 sec and a significant wave height less than about 15 m (assuming a maximum
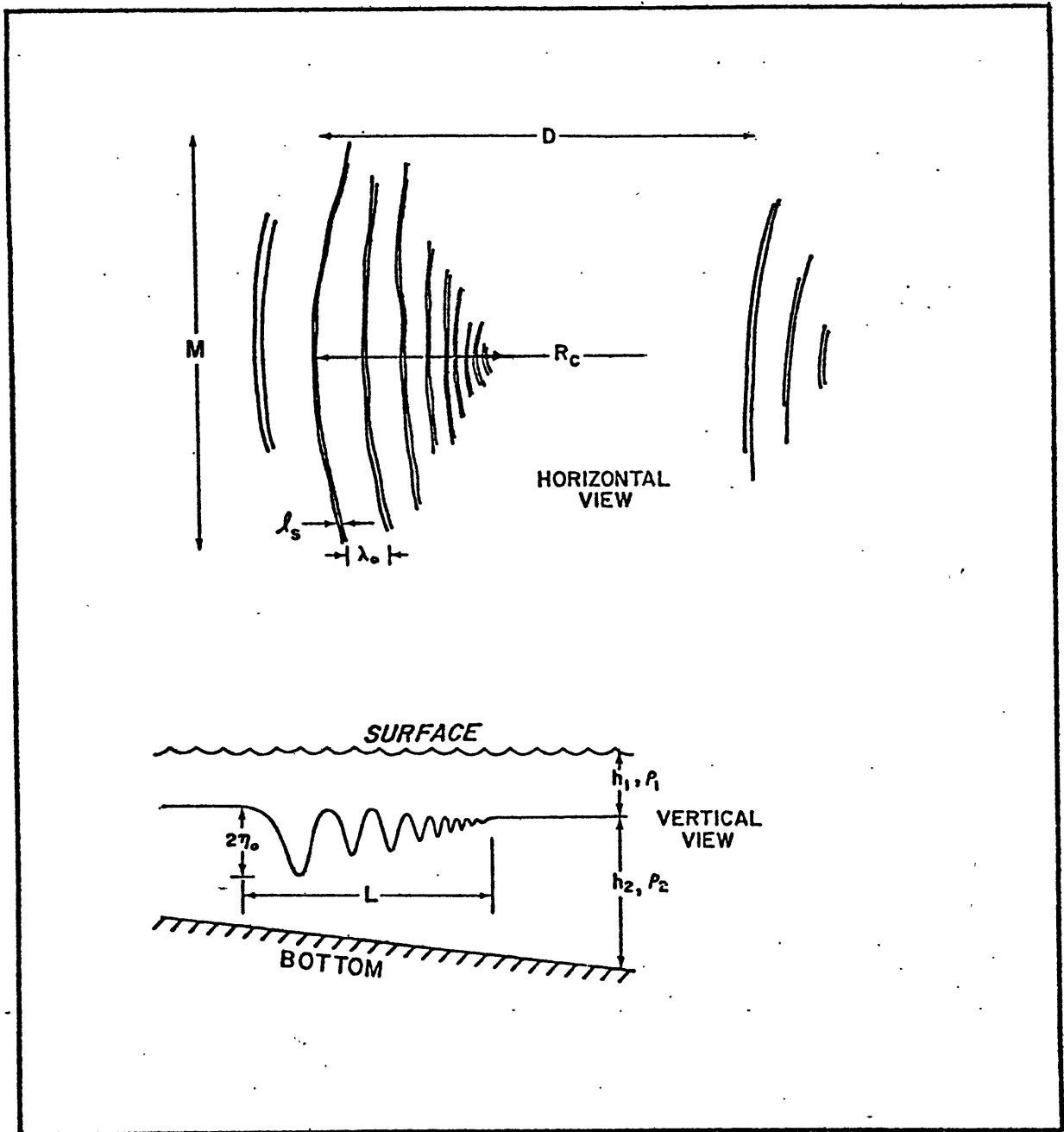
Figure 3.2 - Schematic representation of the parameters in
an internal wave packet (After Apel et al. 1976).

slope of 1:30), weather information for the days registered seas have
been low and the winds light (for an average swell period of 10.5 sec
the wind force must be 12 in Beaufort scale, Defant, Vol II, pg. 62),
thereby eliminating surface waves possibility;

iii) Atmospheric internal waves as defined by clouds are certainly
visible on ERTS-A/B images. For these, the widths of the striations
due to individual clouds are of the order 1/2 of wavelength while the
the pressured ocean striations have widths generally a small fraction
of λ . Furthermore, the latter are most visible when the atmosphere
is most cloud-free.

iv) Film or instrument artifacts have been eliminated by NASA/GSFC
personnel (Apel and Charnel, 1974).

There is also the positive side of the question, that is also listed
in the above referenced paper.

As to the sources and sinks for these internal waves, there is no
doubt that they are "daughter" waves generated for a few hours during
the peak current velocity by the long-wavelength baroclinic tide
occurring at the edges of the continental shelves. They then propagate
with very low phase speeds, of order 0.2 to 0.5 m/sec to be absorbed
in the bottom sediments where the wave breaks on the shelf.

3.2 The Images, Climatological and Ground Truth Data

The primary source of data for the present work was the atlas of
Sawyer and Apel (1976), which contains mozaics of images of LANDSAT
satellite showing internal waves in the eastern coast of the United
States. The images are second generation prints of ERTS images on
photographic film. The scenes showing surface slicks to best advantage
are usually those of channel 6 (600-700 nm) and occasionally channel 7
(700-800 nm). These scenes were enlarged to a scale 1:1,000,000 on
high-contrast emulsion that enhanced the visibility of the slicks
(Apel and Sawyer, 1976). The wave packets are also plotted on a nauti-
cal chart in the same scale as the satellite images.

A total of 78 measurements of the distance between two successive
wave trains were performed. The images exhibiting this phenomenum were
taken during summer months, June, July and August of 1972, 1973 and 1974.

Figs. 3.1a and 3.1b show enlargements of ERTS images where internal
wave packets can be seen. These packets usually appear on the continen-
tal shelf, often in long lines parallel to the slope, leaving no doubt
about their generation.

Since the interest is aimed at possible short-term variations, the
data were divided according to the month of the event. The month of June
had only very few measurements in the last days of the month, so there
we added to the July set of data. For each event a point was selected
such that it was located between the wave trains and at the middle of
the distance D, defined in the previous section. These points are shown
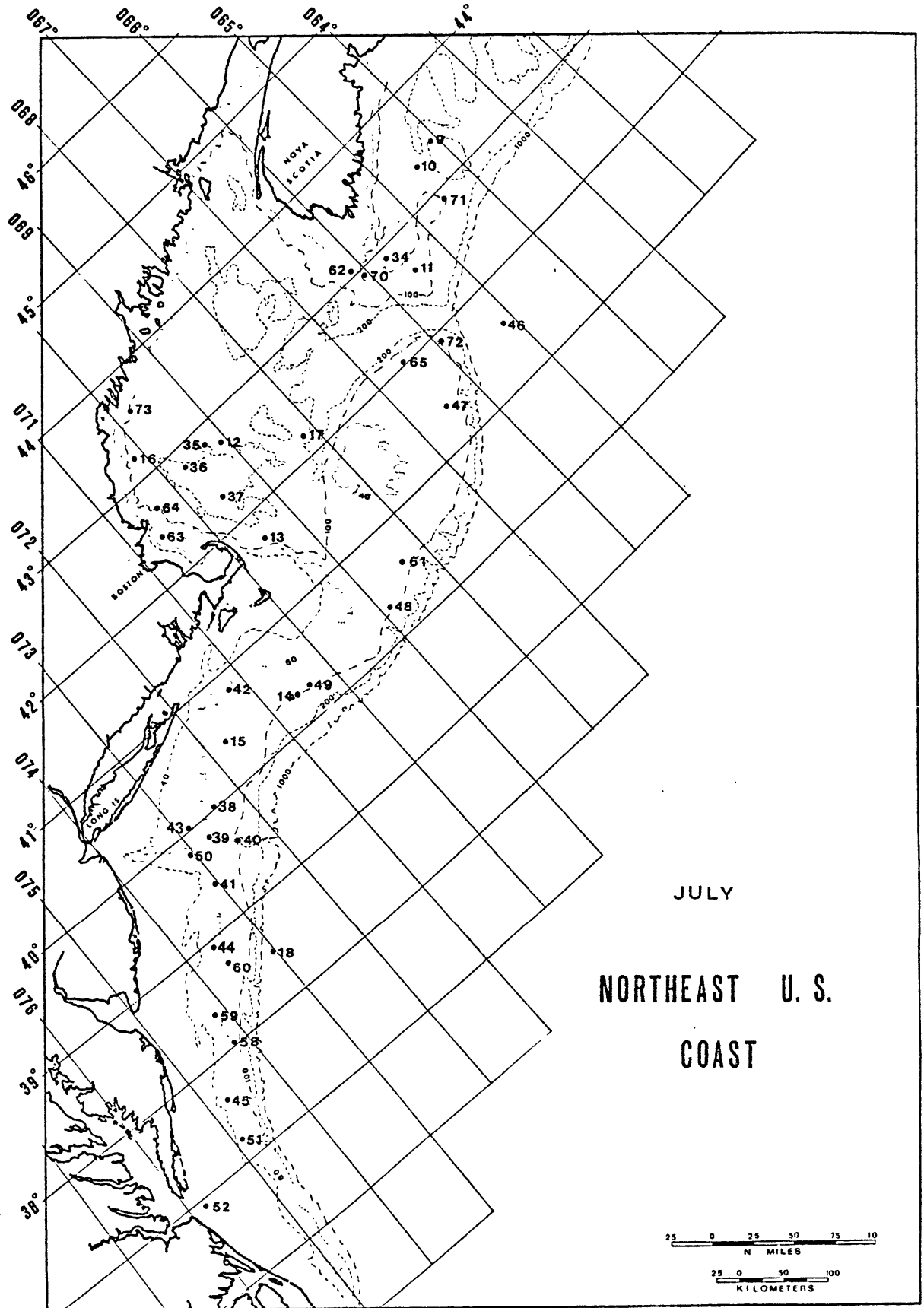in Figs. 3.3 and 3.4 All data are summarized in Table I.

Figure 3.3 - Geographical distribution of internal waves observations
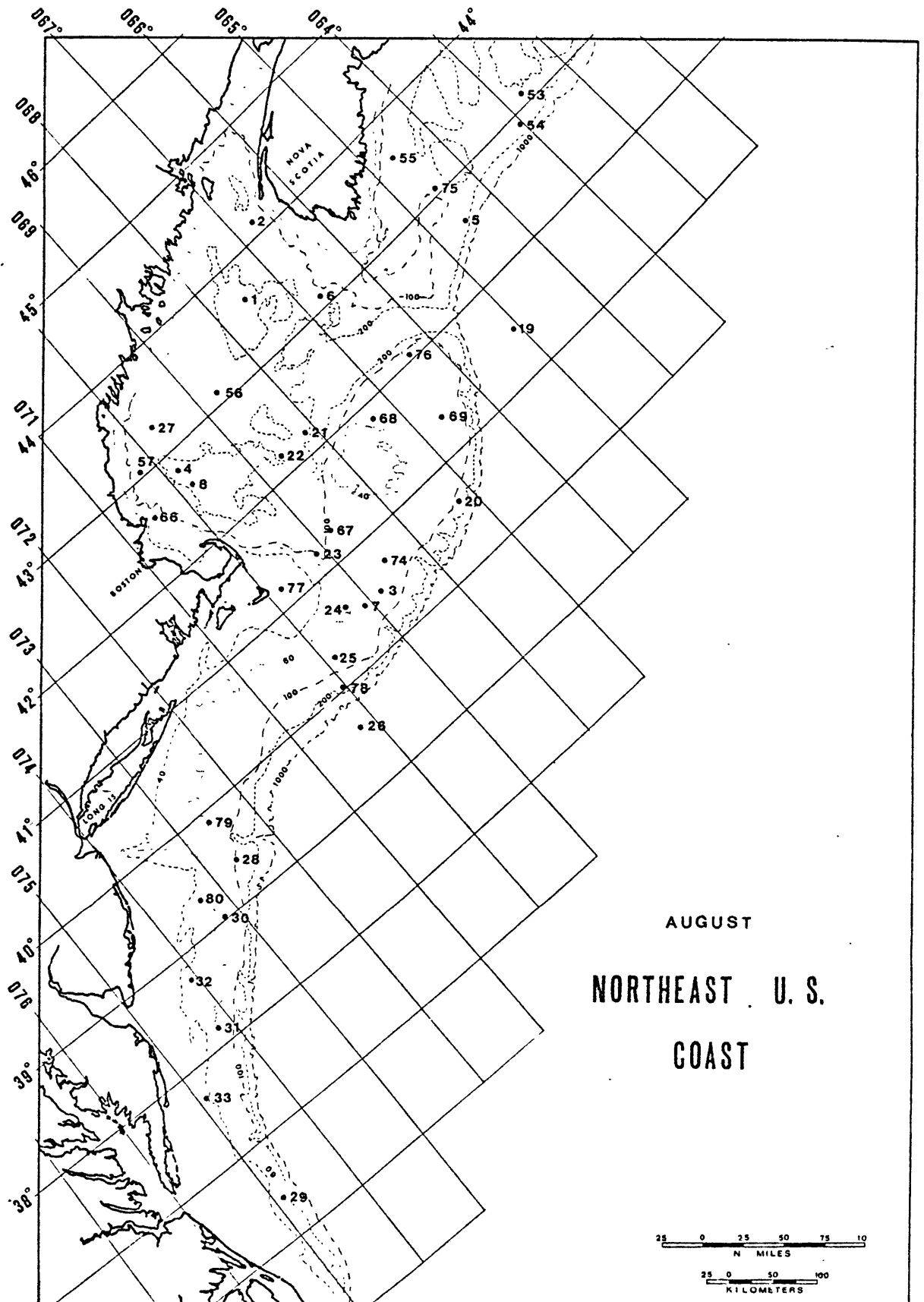for the month of July (1972, 1973 and 1974).

Figure 3.4 - Geographical distribution of internal waves observations
for the month of August (1972, 1973 and 1974).

TABLE I

Summary of observation of internal waves from satellite: Observation
Number, Day of the Year, Latitude, Longitude, Heat Stored Distance
between the Packets, Mixed Layer Depth, and M.L. Depth taking F into account.

OBS.#	MO.DAY.YEAR	LATITUDE	LONGITUDE	AM.HEAT(K CAL/CM^2)	DIST(KM)	M.L.DEP(M)	M.L.D.W/F(M)
1	82074	43.6	67.5	3.6	12.0	7.7	7.7
2	82074	44.2	66.7	3.6	12.0	37.7	38.8
3	82174	40.5	68.8	3.6	12.0	8.4	8.3
4	82274	42.8	69.8	2.5	10.0	6.8	6.8
5	31174	42.6	64.5	3.0	11.0	5.2	5.1
6	80274	43.1	66.7	8.1	18.0	38.6	39.1
7	80374	40.5	69.1	3.6	12.0	4.3	4.3
8	80474	42.6	69.8	2.5	10.0	6.8	6.8
9	71374	43.4	64.1	3.6	12.0	8.8	8.7
10	71474	43.3	64.5	3.6	12.0	8.8	8.7
11	71474	42.6	65.4	6.4	16.0	35.3	35.8
12	71774	42.7	69.1	3.6	12.0	6.2	6.1
13	71774	41.7	69.6	6.4	16.0	24.4	24.4
14	71774	40.3	70.6	4.9	14.0	11.8	11.9
15	71774	40.4	71.7	1.6	8.0	2.7	2.6
17	62874	42.2	68.2	8.1	18.0	20.2	20.4
18	63074	38.5	73.0	8.1	18.0	41.4	41.6
19	80673	41.4	65.1	6.4	16.0	61.0	72.1
20	80773	40.6	67.2	4.9	14.0	22.3	22.3
21	80773	42.2	68.1	4.9	14.0	26.3	26.7
22	80873	42.2	68.6	3.6	12.0	19.3	19.4
23	80873	41.2	69.1	1.6	8.0	8.4	8.4
24	80873	40.6	69.3	3.6	12.0	4.3	4.3
25	80973	40.3	69.9	3.6	12.0	4.3	4.3
26	80973	39.6	70.2	3.6	12.0	8.3	8.3
27	80973	43.3	69.7	2.0	9.0	2.0	2.0
28	81073	39.4	72.6	1.6	8.0	5.8	5.8
29	81173	36.4	74.9	4.9	14.0	10.3	10.3
30	81173	39.0	73.2	3.6	12.0	10.3	10.4
31	81173	38.3	74.2	6.4	16.0	7.2	7.2
32	81173	38.8	74.1	2.5	10.0	2.8	2.8
33	81273	37.7	74.9	3.6	12.0	4.2	4.2
34	71973	42.9	65.7	4.9	14.0	27.0	27.1
35	72273	42.8	69.3	3.6	12.0	6.2	6.1
36	72273	42.8	69.7	3.6	12.0	6.2	6.2
37	72273	42.3	69.6	4.9	14.0	8.4	8.3
38	72373	40.0	72.4	8.1	18.0	8.8	8.8
39	72373	39.8	72.7	3.6	12.0	6.3	6.3
40	72373	39.6	72.4	6.4	16.0	11.3	11.3
41	72373	39.4	73.0	4.9	14.0	7.8	7.8
42	72373	40.8	71.2	3.6	12.0	4.6	4.6
43	72473	40.0	72.9	8.1	18.0	8.8	8.8
44	72473	38.9	73.6	3.6	12.0	18.4	18.4
45	72473	37.6	74.7	3.6	12.0	4.7	4.6
46	70173	41.6	65.2	1.6	8.0	19.7	19.6
47	70173	41.4	66.5	4.9	14.0	10.0	10.0
48	70373	40.3	68.9	1.6	8.0	4.5	4.4
49	70473	40.3	70.4	3.6	12.0	8.8	8.7
50	70673	39.8	73.0	8.1	18.0	12.9	12.9
51	70673	37.2	74.9	3.6	12.0	4.7	4.6
52	70773	36.9	75.8	2.5	10.0	1.9	1.9
53	80972	43.1	62.7	3.6	12.0	5.7	5.7
54	80972	42.9	63.0	3.6	12.0	3.5	3.5
55	81172	43.6	64.7	8.1	18.0	33.3	33.6
56	81372	43.1	68.7	2.5	10.0	8.6	8.5
58	70673	38.1	74.3	3.6	12.0	8.5	8.5
59	70673	38.4	44.2	1.6	8.0	3.8	3.7
60	70673	38.8	73.6	3.6	12.0	18.4	18.5
61	70373	40.6	68.4	4.9	14.0	13.9	14.0
62	71973	43.0	66.1	1.6	8.0	17.7	17.7
63	72273	42.4	70.6	0.6	5.0	0.9	0.9
64	72373	42.7	70.4	2.5	10.0	2.6	2.5
65	71973	42.0	66.5	6.4	16.0	23.1	23.3
66	81073	42.6	70.5	2.5	10.0	3.5	3.5
67	80873	41.3	68.8	4.2	13.0	7.8	7.8
68	80773	41.8	67.3	2.5	10.0	26.2	26.3
69	80673	41.4	66.6	2.5	10.0	19.4	19.7
70	62774	42.9	66.1	3.6	12.0	12.6	12.6
71	71474	42.9	64.5	3.6	12.0	17.5	17.7
72	71474	41.9	65.9	3.6	12.0	44.4	44.7
73	71874	43.6	69.8	2.5	10.0	2.4	2.4
74	80374	40.7	68.5	3.6	12.0	8.4	8.3
75	80174	43.1	64.4	2.5	10.0	10.3	10.3
76	80274	42.5	66.4	6.4	16.0	23.1	23.3
77	80474	41.2	69.8	0.6	5.0	2.1	2.1
78	82274	40.0	70.0	6.4	16.0	11.7	10.6
79	81672	39.9	72.6	2.5	10.0	9.0	9.0
80	81672	39.3	73.3	3.6	12.0	10.3	10.3

The other set of data used was climatological oceanographic data, which comprises mean monthly values of salinity and temperature at standard depths computed for each square of 1° latitude by 1° longitude over the continental shelf from Cape Hatteras to Nova Scotia. Those squares with large number of data were subdivided into four sub-squares of 0.5° latitude by 0.5° longitude. Most of the data was kindly offered by V. Worthington of the Woods Hole Oceanographic Institution.

Missing values at standard depths were replaced by those obtained by graphical interpolation. In few squares we have no values and these were obtained from recent cruises in the months of July and August, through the National Oceanographic Data Center. Among these data is found what can be called ground truth data, i.e. hydrographic data taken at almost the same time as the satellite pass. Two of these are five days apart and the other two are fifteen days apart from the satellite pass. These were the best we could get.

3.3 Preliminary Analysis of the Measurements

The measurements of the distance between successive wave packets taken from the satellite images is plotted in Fig. 3.5 as a histogram with 2 km interval. The distribution obtained suggests at least three dominant spacing multiples of a minimum spacing around 12 km.

The computations of the depth of the mixed layer (h) and of the heat stored (Q) based in the above measurements gave unrealistic results for large spacings, just because h and Q vary as c^2. We could ask - what is going wrong? But remembering that internal wave groups are only visible in surface images in the presence of capillary waves or short
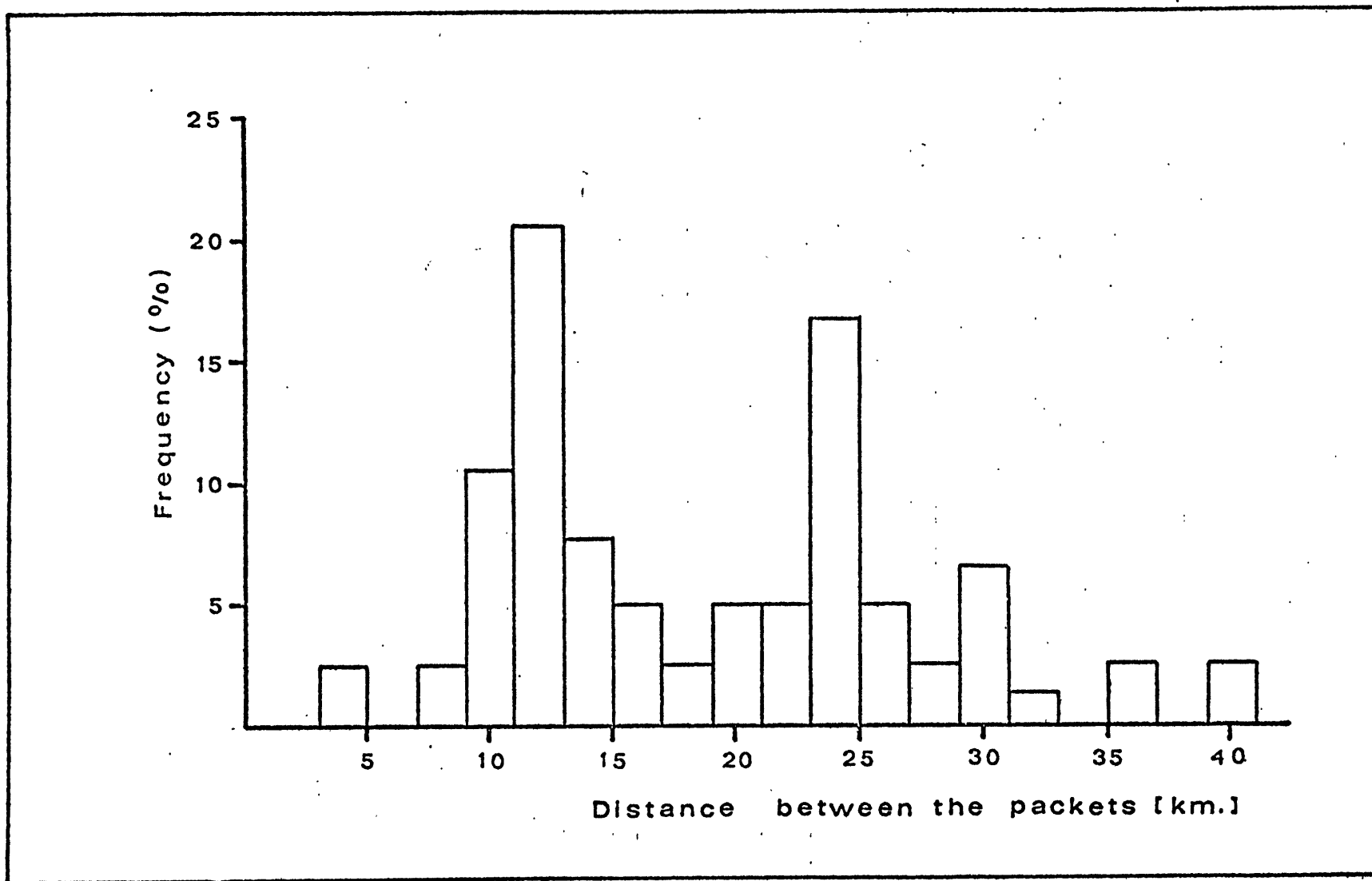
Figure 3.5 - Histogram of the original distances between the
successive wave packets (78 observations).

gravity waves, which only occur when there is wind, (Gargett and Hughes, 1972), the distribution can be interpreted to mean that there is only one wave packet spacing in a given location during the period of the observations. This procedure assumes that the observation of multiple of the minimal group spacing simply means that one has missed some groups since they are not visible because of an absence of surface ripples which can be modified by the internal wave velocity field. On this hypothesis, we assumed that there is a single wave packet spacing, and obtained the histogram shown in Fig. 3.6 including all the wave packets measured.

This interpretation may give an overly provable results, since it supresses variations from the mean longer than the mean, and since such values are modified by the stubraction of a multiple of the mean.

Over the continental shelf typical values for reduced gravity is $g' \sim 0(1)g$ cm^{-3}. For mixed layer depth it is h $\sim$ $0(10^3)$cm. This yields a typical velocity of propagation c $\sim$ $0(30)$cm sec^{-1} and a typical spacing D $\sim$ $0(14)$km.

Another support for the Gausian type of distribution is wave trains found in overlapped satellite images. The ERTS overlapped images are taken 24 hours apart in time. A wave train identified in overlapping images are supposed to be 24 hours apart if there are no topographic features able to generate internal waves in the region. Waves satisfying these requirements were found and the distances between the packets were at least 24 km, corroborating the hypothesis. The values of the depth of the mixed layer and the amount of heat stored were recalculated after this procedure and the new values were quite reasonable.
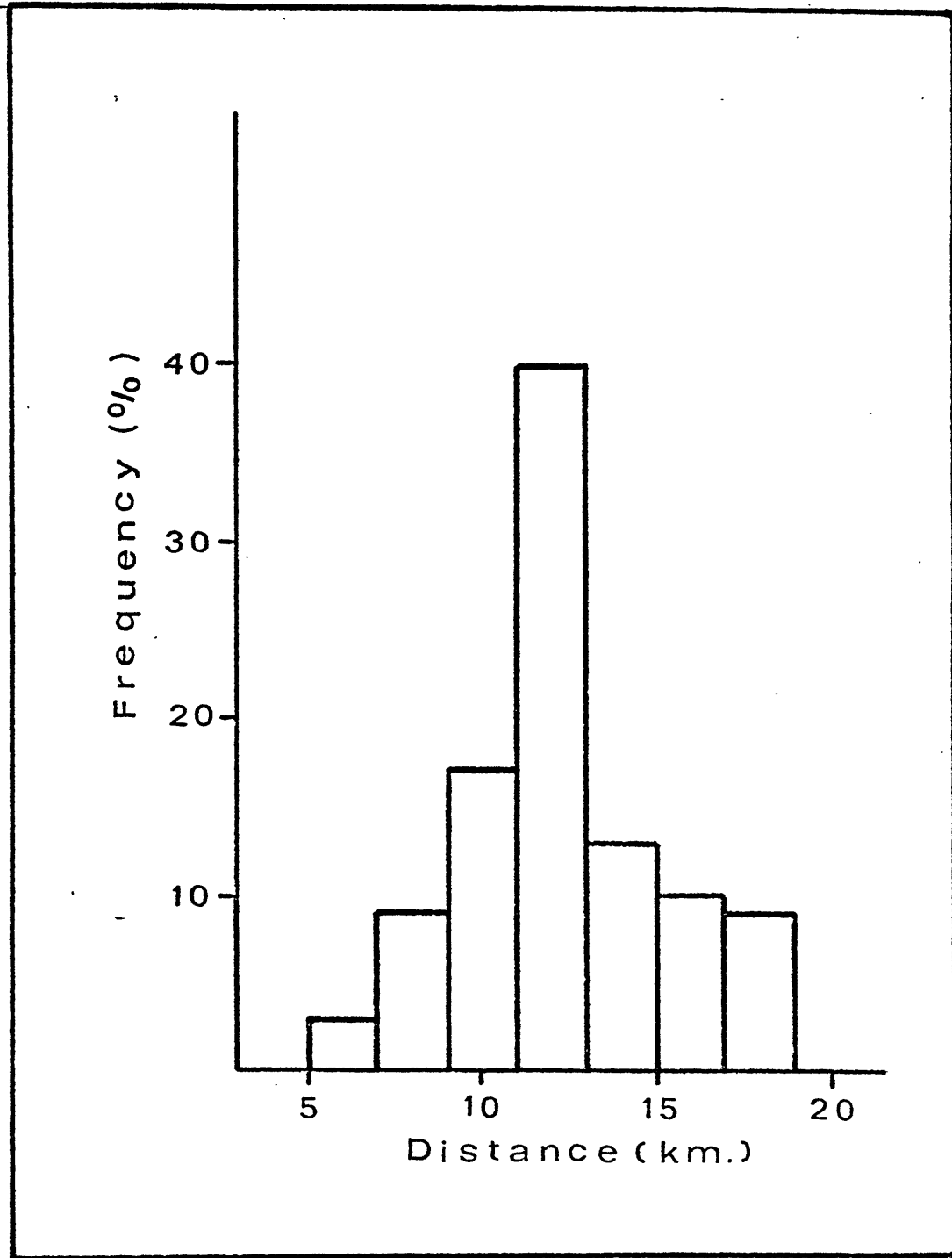
Figure 3.6 - Histogram of the distance between the wave packets
corrected by the multiples of the fundamemtal
minimum distance (78 observations).

4. THE MIXED LAYER DEPTH IN THE OCEANS

4.1 The Stablishing Factors of the Depth of Mixed Layer

In the open ocean there is generally an isothermal surface layer which extends downward from the sea surface. The thickness of this layer is the mixed-layer depth. In a region away from oceanographic boundaries and in the absence of turbulent mixing by strong currents, this depth is assumed to be influenced by two surface-induced processes - wind mixing (forced convection) and convective mixing (free convection). Wind mixing includes all the vertical turbulent mixing processes resulting initially from the transfer of momentum from the wind to the sea. These are the mechanical mixings due to wave action (Laevastu, 1960), turbulent mixing due to the shear of drift currents (Ekman, 1905; Rossby and Montgomery, 1935; Munk and Anderson, 1948), and helical vortices (Langmuir, 1938). Convective mixing occurs as a result of instability created at the surface by surface cooling and by evaporation of fresh water from the sea.

Another surface induced process, if we neglect the effect of diffusion, is the entrainment responsible for the exchange with the water below. The entrainment flow can only be directed towards the more turbulent fluid region, that is, upwards in the present case, cooling and increasing the density of the upper layer. In the absence of entrainment, all the turbulent fluxes become zero at the boundary. This means physically that there is just not enough turbulence energy available to overcome the stable stratification at the base of the layer to produce any mixing with the lower water.

Other factors that can influence the depth of the mixed layer are advection and divergence or convergence due to Ekman transports.

Although it is generally accepted that both forced and free convection are important factors influencing the upper mixed layer, wind mixing can be considered to be the main factor in the considered region and time of the year; convective mixing is assumed to be the secondary. Tabata et al. (1965) showed that there is a linear relation between the mean wind speed averaged 12 hours in advance of the bathythermograph observation and the depth of the summer isothermal surface layer at ocean station P.

In the region considered here the currents over the continental shelf are mainly driven by the meteorological conditions and the drift velocities range from 5 to 25 cm sec^{-1} (Bumpus and Lauzier, 1965), and can be considered weak. We can say that the transport of surface waters have little effect on the properties of the water, but horizontal and vertical mixing are dominant (Ketchum and Corwin, 1964). Thus we can assume the interaction between the sea and the atmosphere to be the dominant factor affecting the upper layers of the ocean in the studied region.

4.2 Estimation of the Mixed Layer Depth

4.2.1 From 2-Layer Model

An application of the results derived in sections 2.1 and 2.2 will be discussed here. The velocity of propagation of the interfacial wave is

$$c^2 = g \frac{\rho_2 - \rho_1}{\rho_2} h_1 \qquad (4.2.1.1)$$

From this relation it is seen that if we know the velocity of propagation c, the density difference $\Delta\rho$, and the density of the lower layer ρ_2, it will be possible to compute the depth of the interface h_1 that we will call mixed layer depth.

The velocity c can be estimated from the distance between two consecutive trains of waves in the satellite images, and assuming they are 12.4 h apart in time (semi-diurnal period), the difference in density $\Delta\rho$ and ρ_2 can be obtained from climatological data. The acceleration of gravity can be assumed to be 980.665 cm sec^{-2}. Table I shows the result of the computation of h_1 using the relation

$$h_1 = \frac{c^2}{g'} = \frac{c^2 \rho_2}{g \Delta\rho} \qquad (4.2.1.2)$$

The same computation of h was repeated, now using the equation

(2.2.12) , that is, the same 2 layer model but taking into account f,

(see also Table I)

$$h_f = \frac{(c^2 - f^2/\alpha^2)^{1/2}}{\alpha c} \coth^{-1} \left[\frac{g'}{\alpha c} \frac{1}{(c^2 - f^2/\alpha^2)^{1/2}} \right]$$

(3.2.1.3)

The values computed using the above equation differ only slightly

from those computed from (4.2.1.2), and for practical purposes they can

be considered equal. So it is perfectly right to neglect f in the

dynamical equations.

Computed values of the depth of the mixed layer were plotted over

a chart of the New England continental shelf for the month of July

and August and are shown in Figs 4.1 and 4.2.

4.2.2 Comparison with Ground Truth Data.

A comparison between the depth of the mixed layer computed using

the expression (4.2.1.1) and the ground truth observations was made.

The closest hydrographic observations performed to the satellite

pass are shown in Figure 4.3. From this figure we can estimate the

depth of the mixed layer. We took as mixed layer depth the depth just

before the pycnocline. Table II shows the results of the comparison.

We must have in mind that the standard depth for sampling in

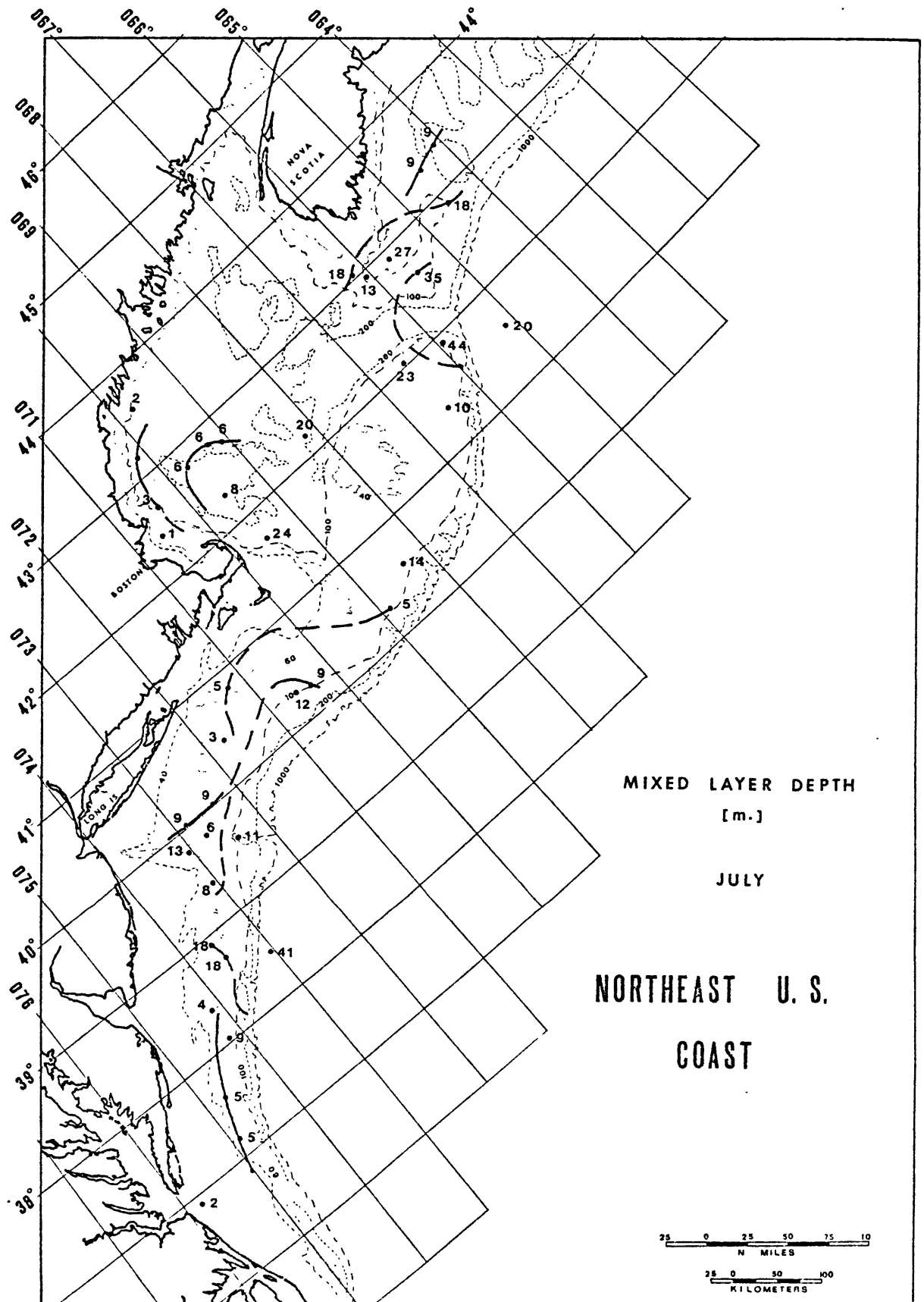hydrography are 0 m, 10 m, 25 m, ... when using Nansem bottles.

Figure 4.1 - Mixed layer depth computed from satellite observations
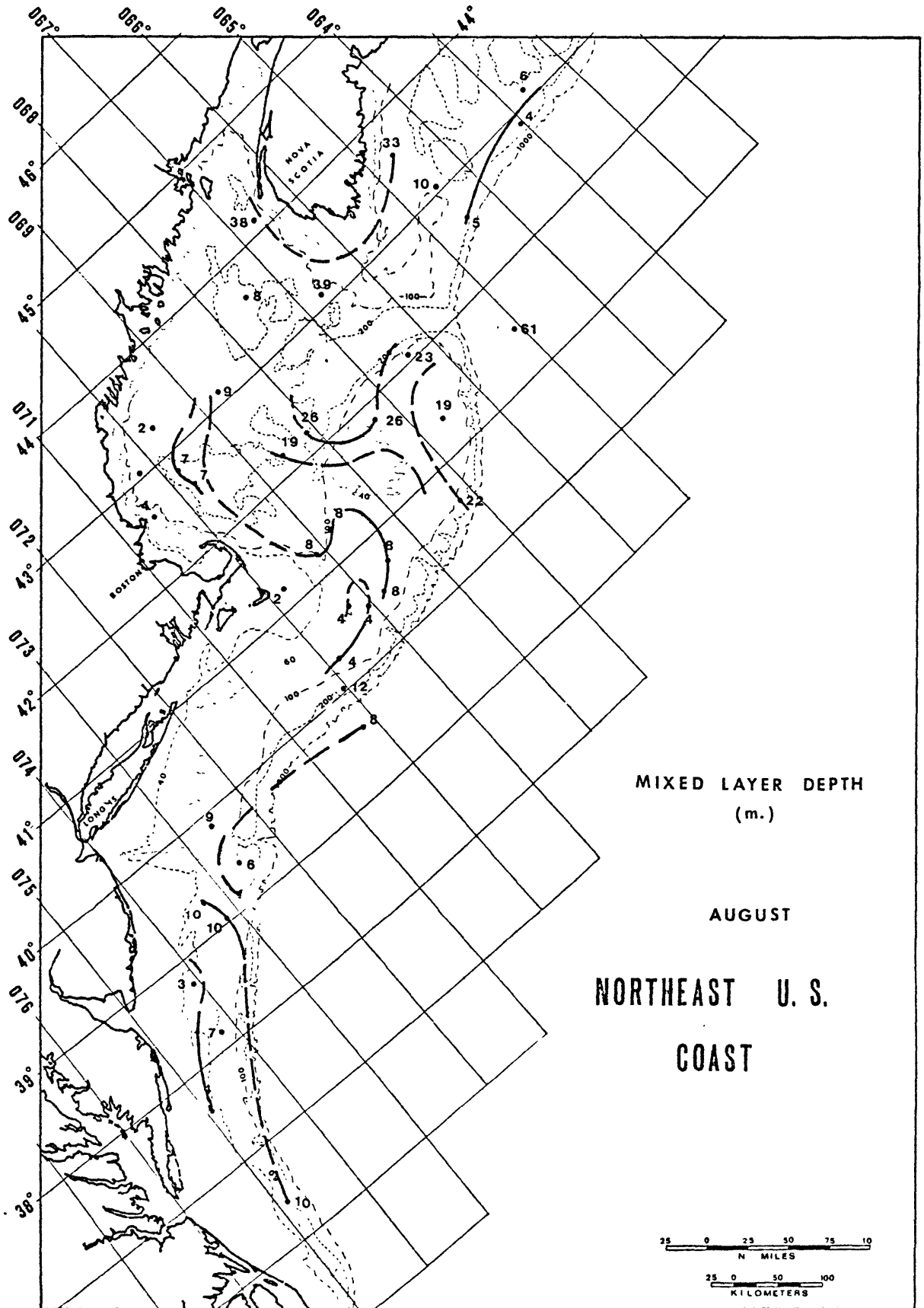of internal waves for the month of July (1972, 1973
anf 1974).

Figure 4.2 - Mixed layer depth computed from satellite observations
of internal waves for the month of August (1972, 1973
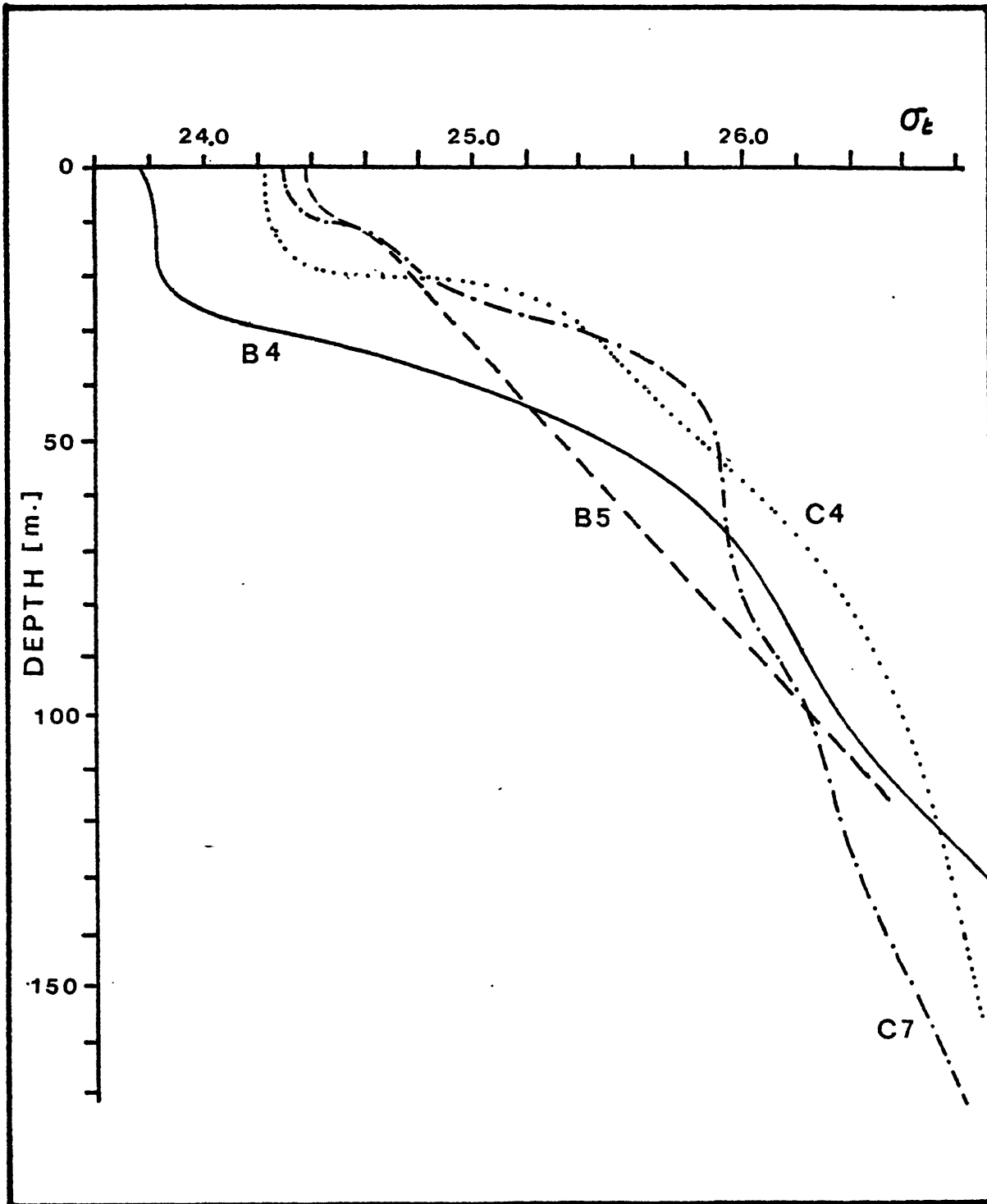and 1974).

Figure 4.3 - Density profiles taken from hydrographic observations used as ground truth.

TABLE II

COMPARISON BETWEEN VALUES OF MIXED LAYER DEPTH (h) AND AMOUNT OF
HEAT STORED (Q) COMPUTED FROM SATELLITE OBSERVATION AND THE CLOSEST
HYDRO COST IN SPACE AND TIME.

	Date	Latitude	Longitude	h (m)	Q (k cal cm^{-2})
sat obs #65	07-19-73	42.01°N	066.30°W	23	6.23
hydro obs B-4	07-14-73	42°26 N	066°13 W	30	9.98
sat obs #70	06-27-74	42.57°N	066.03°W	36	3.51
hydro obs C-7	07-11-74	43°03 N	066°53 W	26	5.04
sat obs #62	07-19-73	43.02°N	066.06°W	10	1.56
hydro obs B-5	07-14-73	42°42 N	066.40 W	9	3.56
sat obs #76	08-02-74	42.50°N	066.40°W	24	6.24
hydro obs C-4	07-13-74	42°31 N	066°11 W	20	9.30

Consequently if we have a sharp pycnocline between 0 and 10 meters

we can not recognize it by plotting the standard depth values. This

means that a lower value of mixed depth layer, computed by (4.2.1.1),

could be hidden in the ground truth data due to the coarse sampling points.

5. THE AMOUNT OF HEAT STORED IN UPPER LAYERS OF THE OCEAN

5.1 The Role of the Stored Heat

An extremely important component of the earth's heat balance is

the storage of heat in the summer hemisphere and its release in the

winter hemisphere. Except in certain land areas where a considerable

seasonal fluctuation in soil moisture takes place, heat storage is

severely limited by the comparatively slow rate of heat conduction in

the solid earth. The relatively low heat capacity of air restricts

seasonal heat storage by the atmosphere. The hydrosphere, on the

other hand, is partly transparent to short-wave radiation, has a great

heat capacity, and is in nearly constant turbulent motion. It is

able, therefore, to play a dominant role in seasonal heat storage.

The heat stored in the seasonal upper warm layer of the oceans

comes from solar radiative input and is in part balanced by losses

to the atmosphere in the form of radiation and diffusion of sensible

heat and latent heat of evaporation, as well as turbulent exchanges

with deeper layers of the ocean. These processes, balanced by hori-

zontal advection, determine the temperature, depth and the salinity

of the upper layer, the time of layer formation in the spring, and the

overturning and disappearance of the layer in late fall.

The heat stored in the upper ocean affects, both climatologically

and synoptically, the weather development and the mixing processes

in the layer driven by wind and thermal effects also transport oxygen,

nutrients and biota. Observations indicate that seasonal heat storage

takes place in the upper one hundred to one hundred and fifty meters

of the ocean.

5.2 Heat Stored Calculations from In-Situ Measurements

The heat flux from the atmosphere through the sea surface ends up
in different ways:

a) it may raise the temperature of the ocean column,

b) it may be carried away by horizontal advection, or

c) it may be exchanged with deep colder layer.

The above processes actually occur simultaneously in the ocean.

The annual heating cycle of the water column over the continental
shelf is well known, and as examples we have Figures 5.1a, 5.1b and
5.1c. These figures show the variation of the mean monthly values of
temperature of the upper water column from the early spring to late
summer for three representative regions of the eastern continental
shelf. These regions cover three squares where we have some internal
wave observations. Figure 5.1a shows the temperature profiles for the
square (42-43)°N x (065-066)°W, covering the entrance and the north
part of the Northeast Channel, Gulf of Maine. Figure 5.1b shows the
profiles for the equare (40-41)°N x (068-069)°W, covering the region
of the continental shelf and continental slope east of Cape Cod.
Figure 5.1c shows profiles of the equare (37-38)°N x (074-075)°W
covering the continental shelf and slope off Delaware and Maryland.

From these figures we notice that the water is heated from a
minimum temperature profile $T_0(z)$ (March), to a maximum profile that
could be August or September. As already pointed out in Chapter 5
we can neglect the advected heat, and here we are also going to neglect
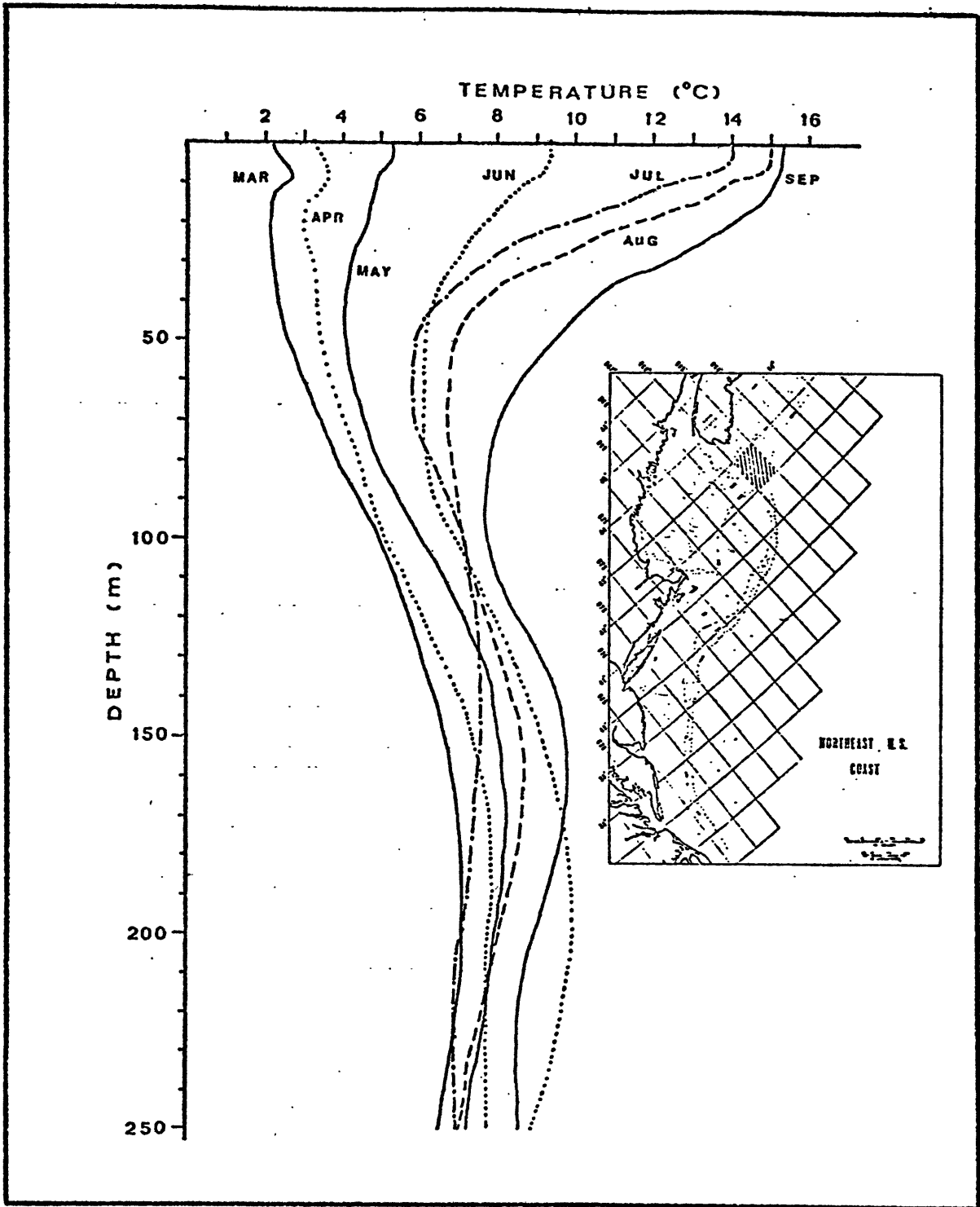the exchange with the water below. We can then define the amount of

Figure 5.1a - The annual heating cycle of the upper ocean
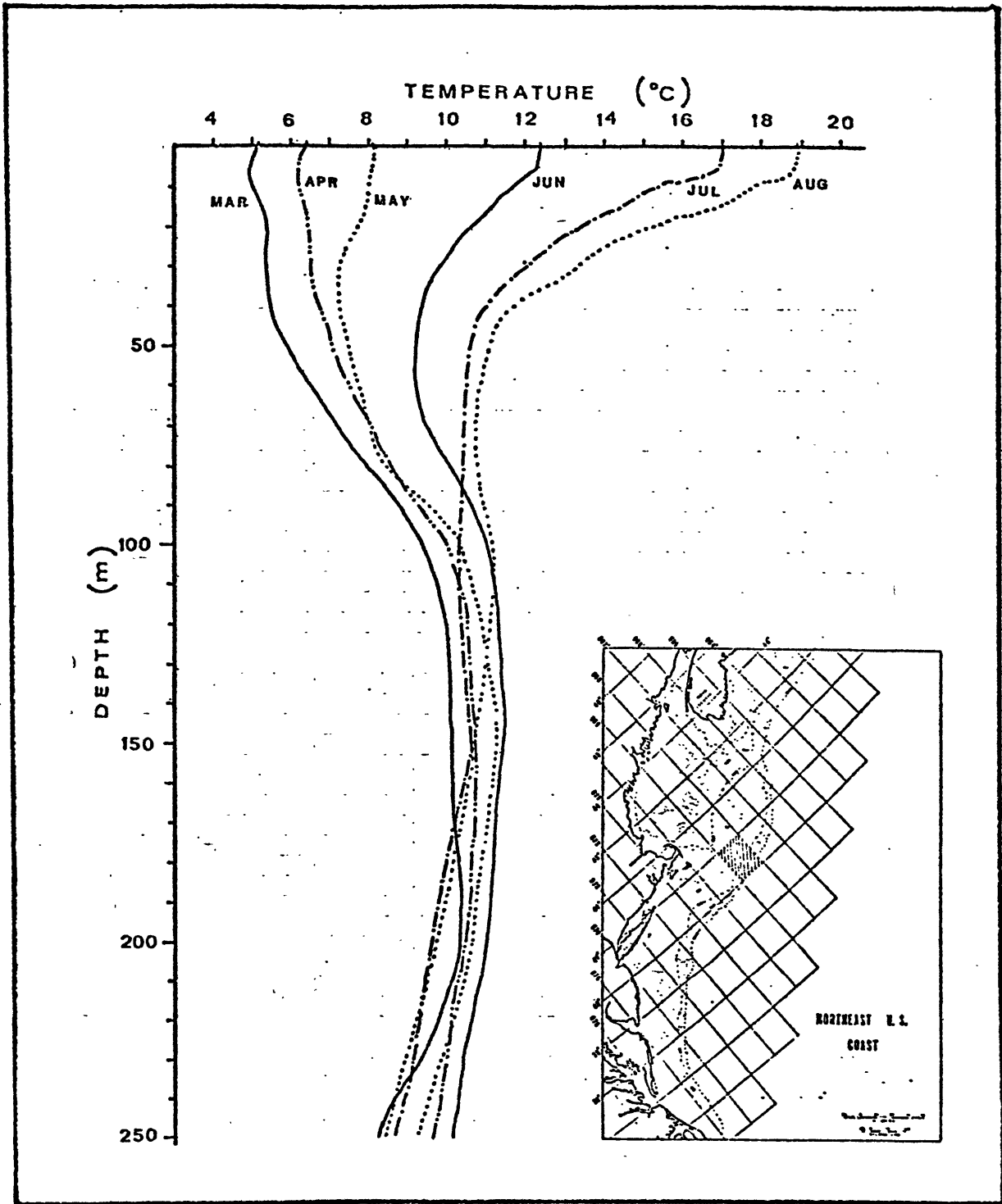from the region (42-43)°N and (065-066)°W.

Figure 5.1b – The annual heating cycle of the upper ocean for
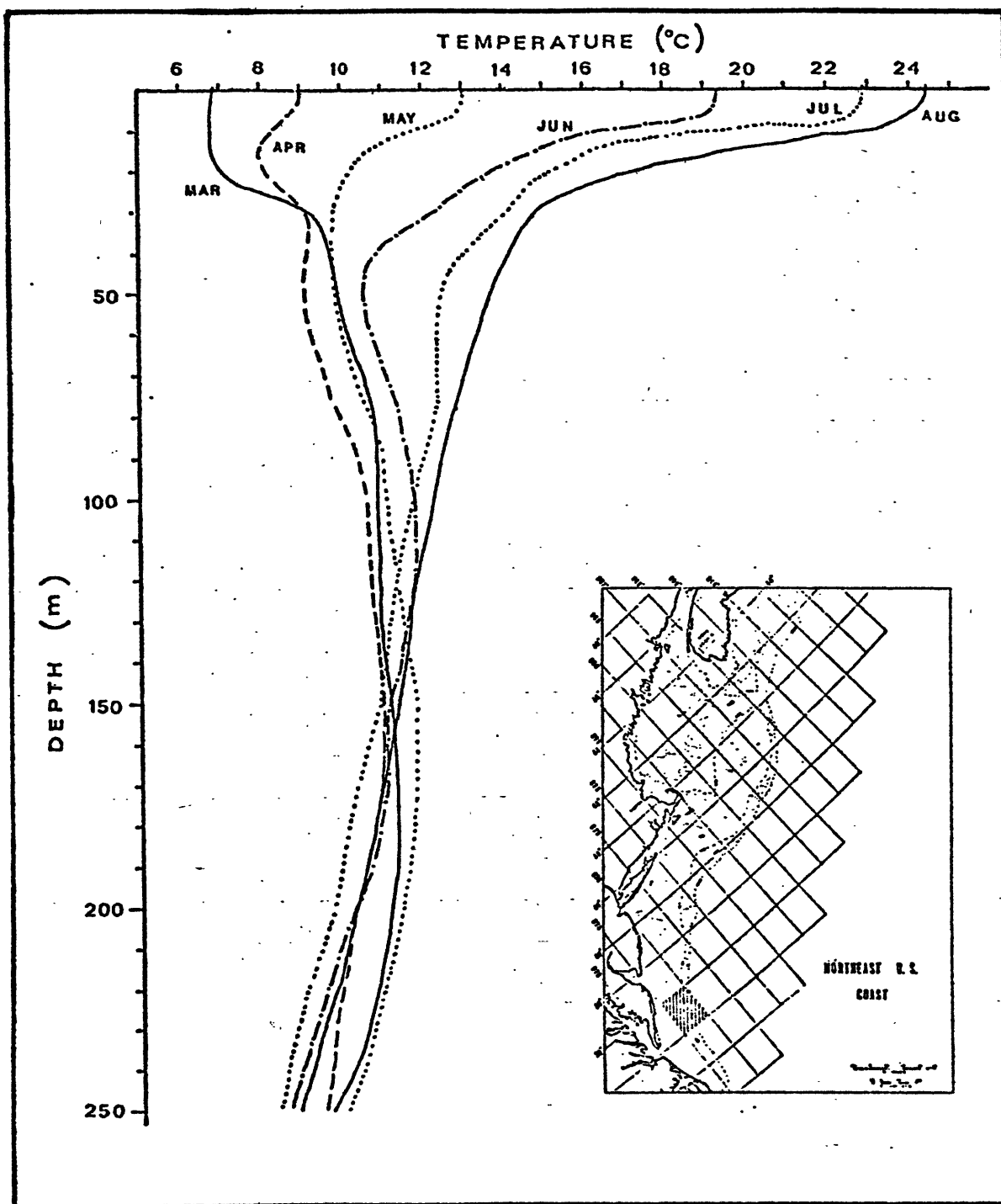the regions (40-41)°N and (068-069)°W.

Figure 5.1.c - The annual heating cycle of the upper ocean for
the region (37-38)° and (074-075)°W.

heat contained in the upper layer of the ocean as the heat accumulated from the minimum temperature profile $T_0(z)$ to a given profile $T(z)$ in absence of advection and exchange with water below as

$$Q_s = \int_{-h}^{0} \rho \, c_p \left[T(z) - T_0(z) \right] dz \quad , \tag{5.2.1}$$

where ρ is the density of the sea water, c_p is the specific heat at constant pressure and h is the depth of the thermocline. When using this definition we must be aware that we are overestimating its value. To overcome this overestimation instead of using $T_0(z)$ for the month of March, we have chosen the minimum profile two months latter.

5.3 Heat Storage Calculations from Satellite Images

5.3.1 Based on Two-Layer Model

The most important application of the internal wave images from satellites is without doubt the fact that we can actually compute the amount of heat stored in the upper layer using only the velocity of propagation of the packets. Let us see how this can be done. Start with the amount of heat stored defined as

$$Q = \rho_1 \, c_p \, \Delta T \, h \quad , \tag{5.3.1}$$

Now we rewrite our equation of state (1.2.13) assuming that the changes

in salinity are negligible when accounting for changes in density, and

since we are dealing with a two-layer ocean,

$$\rho_1 = \rho_2 \ (1 - \alpha \Delta T)$$

(5.3.2)

The above assumption is critical because in estuaries, for example,

the density is controlled mainly by the salinity gradient.

Figure 5.2 is a plot of values of $-\alpha\Delta T$ against $\beta\Delta S$, for the regions

shown in the chart inside the figure. Besides the point drawn as an

open circle, the other points indeed support the assumption that $\beta\Delta S$

is not so important as $-\alpha\Delta T$ in account for density changes.

The anomalous point describes the density changes for the coastal

region east of Delaware, being under the influence of the Chesapeake

Bay waters. Since we did not plot points for all regions we can expect

the same behavior for coastal regions in the vicinity of large river

mouths. Fortunately there are very few internal wave observations

under such conditions. After all, these regions are no problem because

we can overcome this fact by taking into account the salinity dependence

by determining a function g=g(T,S) through a T,S relationship for these

regions and still keep a linear dependence on temperature. This proce-

dure would also improve the determination of the density in other

regions. From (2.1.7)

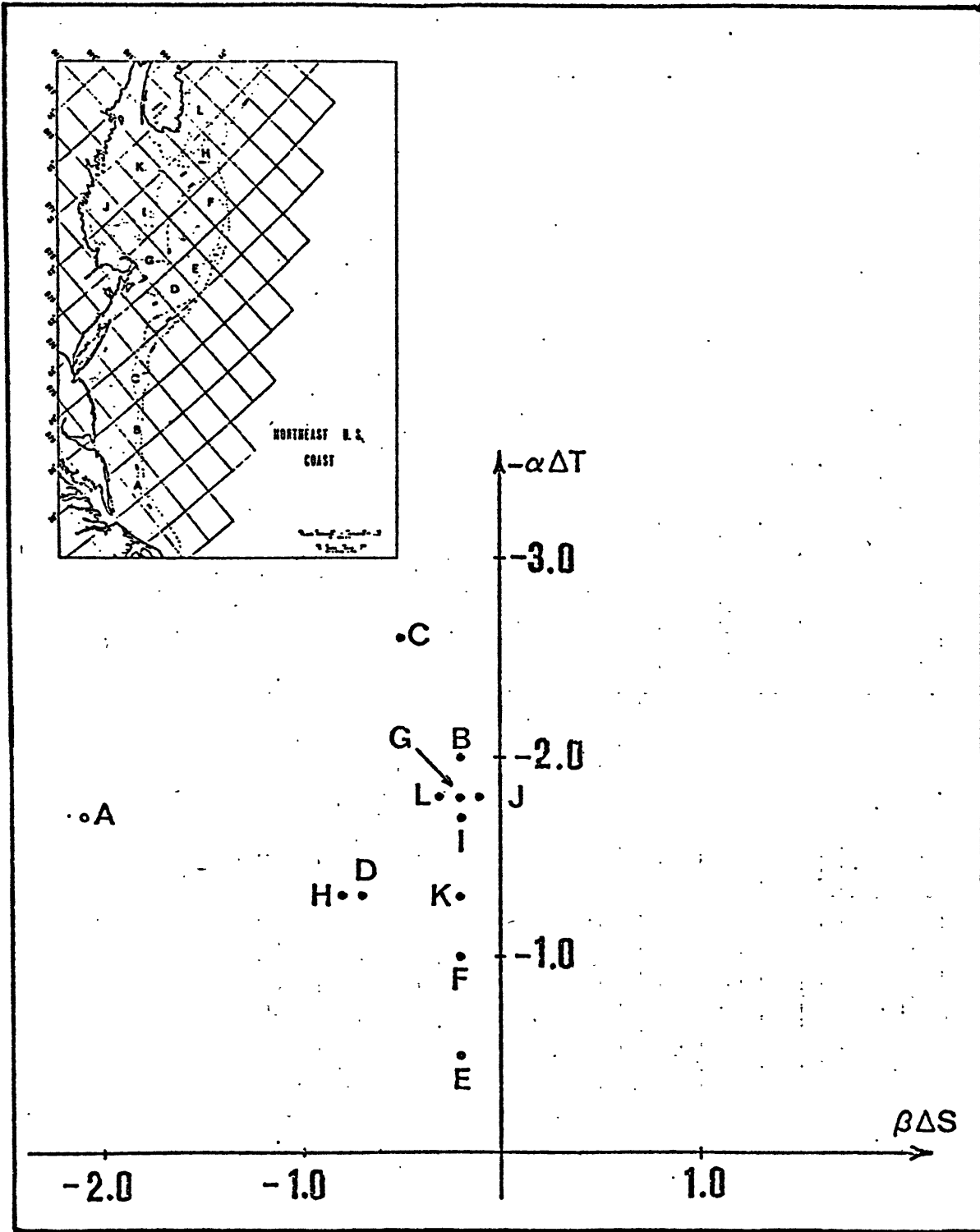$$\frac{\Delta\rho}{\rho_2} = \frac{c^2}{gh}$$

(5.3.3)

Figure 5.2 - Values of $-\alpha\Delta T$ and $\beta\Delta S$ from mean monthly
values of T and S for the regions shown
in the chart.

from (5.3.2)

$$\frac{\Delta \rho}{\rho_2} = \alpha \Delta T \qquad (5.3.4)$$

Combining the relations (5.3.4), (5.3.3) and (5.3.1) and also assuming $\rho_1 \approx \rho_2$, which numerically will not make any computational difference, we get

$$Q = \frac{\rho_2 \, c_p \, c^2}{\alpha \, g} \qquad (5.3.5)$$

The expression (5.3.5) gives us in cal cm^{-2}, if we use cgs units, the amount of heat stored in the upper layer, under the above assumptions. Assuming c_p, g and α constants, the only variables are c^2, that is measurable from satellite images, and ρ_2 that can be inferred from climatological data.

The motivation to use ρ_2 instead of ρ_1 is that, although both are of order 1, the former one is less subject to small term variations than the last one.

The comparison with the scarce ground truth data available is shown in Figure 5.3. The values of heat stored inferred from satellite observations are less than the one computed from in-situ data and this will be discussed later. Charts of the heat stored in the upper layer over the New England continental shelf for the month of July and August are shown in Figures 5.4 and 5.5.
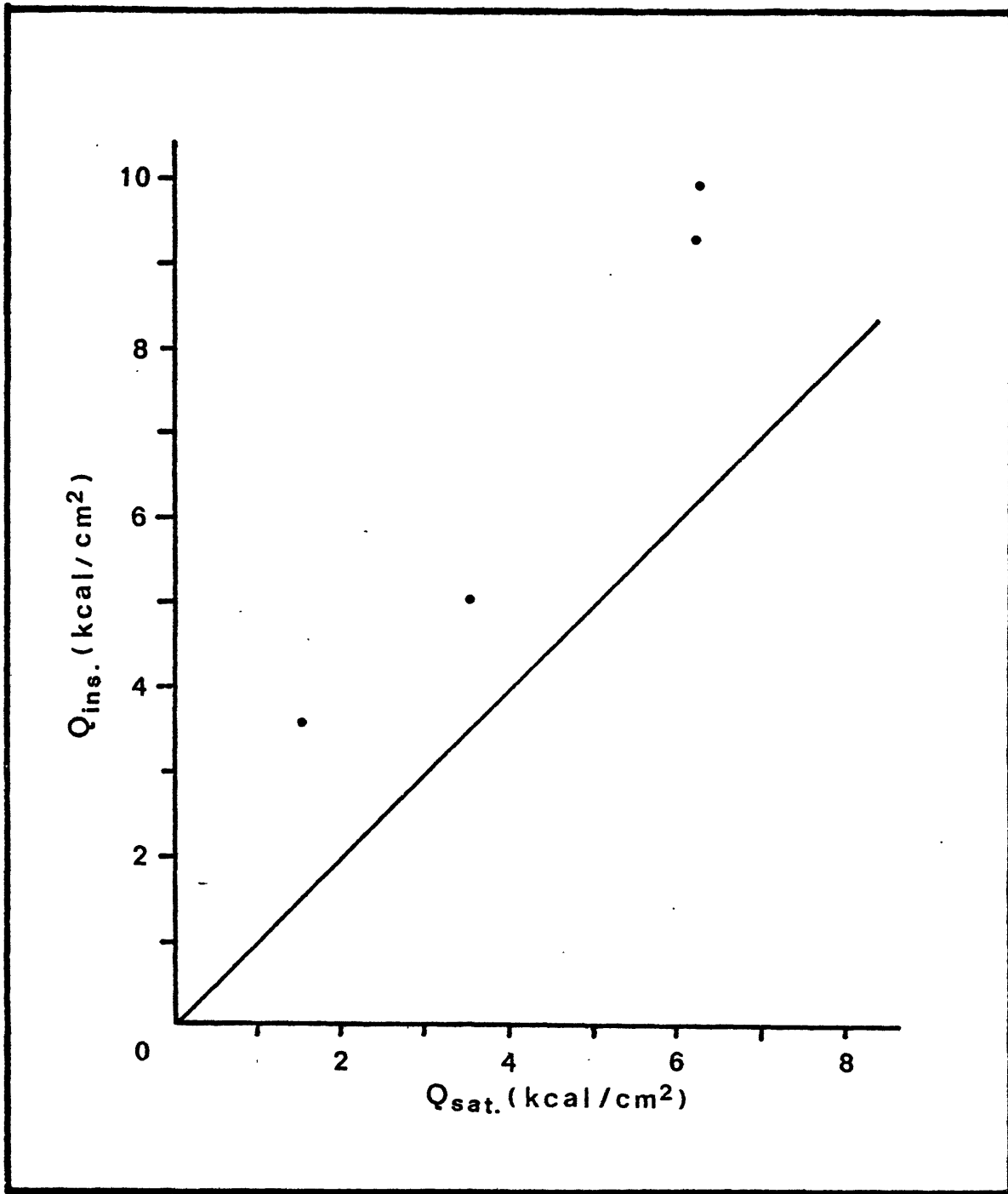
Figure 5.3 - Comparison of stored heat computed from satellite
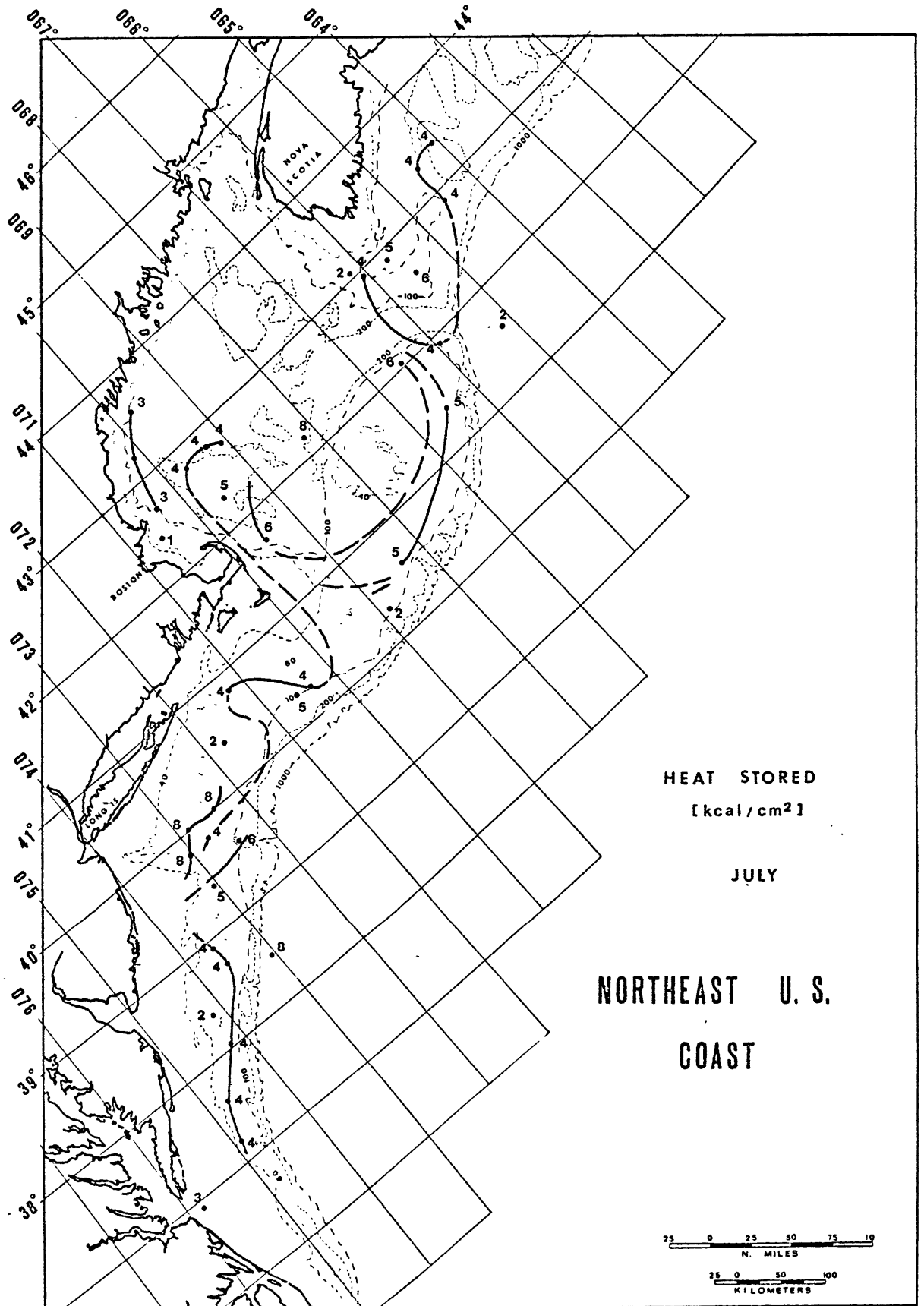observations (Q_{sat}) of internal waves and those
computed from in-situ data (Q_{ins}).

Figure 5.4 - Amount of heat stored computed from
satellite observations of internal
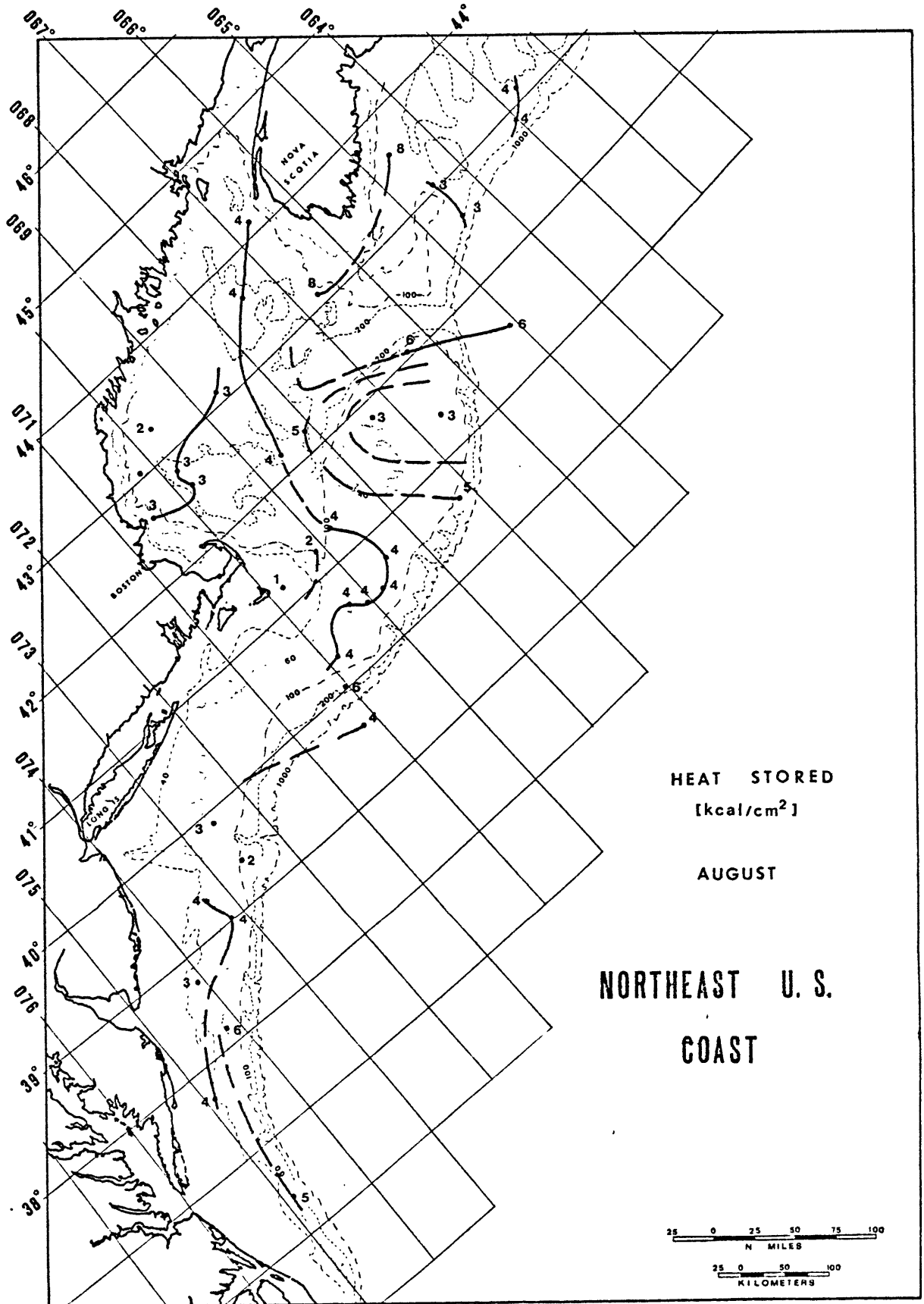waves for the month of July.

HEAT STORED
[kcal/cm²]

AUGUST

NORTHEAST U. S.

COAST

Figure 5.5 - Amount of heat stored computed from satellite
observations of internal waves for the month
of August.

6. RESULTS

6.1 The Accuracy and Dispersion of Q and h.

The scope of the work is not to verify the accuracy of the distance

between the packets, but to show that these measurements can be used

to compute mixed layer depth and amount of heat stored. Due to the

nature of the experiment discussed here, that is, measurements scattered

in space and time, it is rather difficult to discuss accuracy of the

extimates of h and Q. To get an estimate for this accuracy, we are

going to make a simple analysis of error in the analytic expressions

for Q and h. From the measurements we can attribute a fractional error

of 0.5 km or 4% relative to the mean value in the determination of the

spacing D. Since we are using climatological mean values of $\Delta\rho$ and ρ,

we are not going to use the error in the computation of ρ from in-situ

measurements but rather the dispersion around the mean value. This

yields respectively a fractional error of 0.07% for ρ_2 and 40% for $\Delta\rho$.

Taking the expression for Q as

$$Q = \frac{c_p}{g \alpha T^2} \beta_2 D^2 = k \beta_2 D^2 \qquad (6.1.1)$$

the fractional error will be at worst conditions:

$$f_Q = 8.1 \%$$

Simularly using the expression for h as

$$h = \frac{D^2 \rho_2}{g T^2 \Delta \rho} = k \frac{D^2 \rho_2}{\Delta \rho}$$

(6.1.2)

the fractional error in h will be at worst

$$f_h = 32 \%$$

In order to enhance time variability an analysis of the dispersion of the variables about the mean value was done for each month separately, and the results are shown in Table III. From (6.1.1) we see that only two quantities contribute to a dispersion in Q. These are the distance between the packets D and the bottom density ρ_2. The fractional standard deviation of Q is

$$\frac{\sigma_Q}{\bar{Q}} = \left[4 \frac{\sigma_D^2}{D^2} + \frac{\sigma_{\rho_2}^2}{\rho_2^2} \right]^{1/2} \simeq 2 \frac{\sigma_D}{D}$$

or using the values of Table III, $\sigma Q / \bar{Q} = 0.51$ (for July) and the standard "error" of the mean will be .34, a value that agrees well with the one calculated from the statistics of the data. The same applied to h yields

$$\frac{\sigma_{h_1}}{h_1} = \left[4 \frac{\sigma_D^2}{D^2} + \frac{\sigma_{\rho_2}^2}{\rho_2^2} + \frac{\sigma_{\Delta\rho}^2}{\Delta\rho^2} \right]^{1/2} \simeq \left[4 \frac{\sigma_D^2}{D^2} + \frac{\sigma_{\Delta\rho}^2}{\Delta\rho_2} \right]^{1/2}$$

TABLE III

STATISTICS OF THE PARAMETERS MEASURED IN THE IMAGES, OBTAINED FROM CLIMATOLOGY

AND COMPUTED FROM THE TWO-LAYER MODEL

Parameter	June/July (40 data)			August (38 data)		
	mean	stand. dev.	sd. error mean	mean	stand. dev.	sd. error mean
Distance between the packets (km)	12.6	3.2	0.1	11.9	2.7	0.44
Bottom density (g cm^{-3})	1.02384	0.00075	0.00012	1.02383	0.00090	0.00015
Density difference (g cm^{-3})	0.00104	0.00059	0.00009	0.00095	0.00058	0.00009
Amount of heat stored (k cal/cm^2)	4.2	2.0	0.32	3.7	1.7	0.28
Mixed layer depth (m)	13.0	10.4	1.24	13.0	12.6	2.04

and a value of $\sigma h_1/h_1 = 0.76$ or a standard "error" of the mean 1.56. We found similar agreement for the same quantities computed for the month of August.

The dispersion in h is enormous and among the reasons for this we can mention large variations of the mixed layer depth due to the internal tides and the high dispersion in $\Delta\rho$. This value is sometimes subjected to large variations in a time scale smaller than a month. The difference between the mean values of mixed layer depth and amount of heat stored for July and August was not found to be significant. This would be expected since these values were averaged over a month and over a large area.

6.2 Discussion of the Results for a Two-Layer Model

6.2.1 Mixed Layer Depth

The computation of the mixed layer depth (h) using (4.2.1.2) rely

on the measurements of distance D and on the climatological values

of $\Delta\rho$. While the former has a percentage error of 4% the last one

has an error of 40%. The propagation of error analysis gives an error

of 32% in the estimation of h. Table II shows a comparison of h

computed from satellite and taken from in-situ hydrographic cast. In

three out of four observations the satellite estimation gives deeper

values than the hydro cast. Here actually we cannot take the hydro

cast values as standard for comparison because first, they were not

taken at the same time, and second, because of the effect of the internal

tide over the sampling.

Halpern's data (1971) show that the apparent depth of the upper

layer may vary by 30% or more during a tidal period. Rattray (1969)

and Halpern (1971) have shown that the internal tide propagates on the

seasonal pycnocline as a wave packet, the front of which starts with

a depression of the thermocline, followed by a series of undulations

which leaves the pycnocline lower than ahead of the wave packet. The

pycnocline then slowly rises to reach its maximum height just before

the wave packet belonging to the succeeding tide arrives. The effect

of this over the observations taken in a hydrographic station can be

foreseen since the amplitude of the waves range from 4 to 20 m in

crest-to-trough distance. It should be pointed out that the error in

the observations would probably be more serious for STD casts than for

Nansen casts, because an STD cast is a near-instantaneous profile of temperature and salinity, whereas Nansen bottles are allowed to "soak" at a given depth and provide an average temperature over about a 10 min. interval (R. Williams and F. Godshall, 1977). Figure 3.3 shows a schematic drawing of this wave packet.

Generally speaking, the mixed layer depth charts show deeper values for July. The reason for this is that in July the winds are stronger than in August (Navy Hydrographic Office, 1959). There is a general tendency of h to get shallower shoreward. Unusual deep values are observed on the Nova Scotia coast in August. Deep values of h are expected over the Banks region due to the wind mixing.

To have an idea of the possible one month time variations we choose the spatially closest repeated observation we have, and the comparison is made in Table IV. There is one observation off the continental shelf (Obs #19, 46) and probably the generation mechanism is the same as those over the continental shelf, so we can consider the same population's data. This observation gives a much deeper value for August than for July.

Usually in open ocean we find deeper values of mixed layer depth than over the continental shelf. It seems that the free convection also plays a more important role here.

Two of the values in Table IV show that differences within the limit of accuracy are not actually one month apart. They are around fifteen days apart so they cannot be considered representative.

.

TABLE IV

ONE MONTH VARIATION IN MIXED LAYER DEPTH AND AMOUNT OF
HEAT STORED FROM SATELLITE INTERNAL WAVE OBSERVATION

MONTH	OBS.#	h(m)	Q(k cal/cm^2)
July	46	20	1.6
August	19	61	6.4
July	65	23	6.4
August	76	23	6.4
July	61	14	4.9
August	74	8	3.6
July	47	10	4.9
August	69	19	2.5
June	17	20	8.1
August	21	26	4.9
July	45	5	3.6
August	33	4	3.6

The effect of the inclusion of the Coriolis parameter in the computation of the mixed layer is shown in Table I. As pointed out before, it is negligible because the correction term f^2/α^2 is small compared to c^2; it varies from 1 to 10. Meanwhile c^2 is of order 10^3.

6.2.2 Amount of Heat Stored

Unlike the mixed layer depth, the computation of the amount of heat relies only on D, consequently the propagation of error analyses yield and error of 8% for Q. The comparison with the available ground truth shows that the heat stored computed from satellite is lower than those computed from in-situ hydrocast. This is due to the fact that at the leading wave of the group the pycnocline is shallower.

The heat storage charts show the unexpected result that in some regions the values of stored heat are larger in July than in August. A possible reason for this anomalous result is air sea interaction. During July in the Gulf of Maine there is fog, mostly in the night and early morning, that acts as a radiative blanket reducing losses by radiation. It also functions as an evaporation shield preventing the increasing loss of sensible heat by evaporation. In August the fog is reduced and the losses are increased.

In the one month variation Table IV the observation outside the continental shelf (obs. #46,19) follow the general trend of higher values of Q for August than July.

6.3 Additional Comments

Some questions arise from the results discussed in the previous sections.

a) Under which conditions do the two methods of calculating heat storage give comparable results?

b) What is the real depth of the layer?

c) Can short term variations of the mixed layer depth induce variations in the amount of heat stored?

d) How large are these variations?

Let us try to comment on the above questions.

a) The expression giving Q from in-situ measurements (5.2.1) is an integral that involves time, while equation (5.3.5) does not. In order to compare the computations we have to assume $T_o(z)$ constant. This means that the deep water temperature is constant all year. The recalculation of Q using the assumption T_o = const. yields values closer to those computed from satellite data.

b) Since we have measured the distance between the leading waves of the packets we are assuming the depth at this point, i.e., shallower than the observed in-situ, as already discussed. This depth is going to vary from the leading wave to the back of the packet, and the point plotted in the charts would have to be shifted a half spacing backward or forward. The only way to compare the depth of the mixed layer discussed here is to moor a buoy with temperature sensors at a geographical location chosen on the basis of satellite image.

c) The amount of heat stored in the upper layer is subject to diurnal variations due to the heating during the day and cooling during the night.

The internal waves only redistribute the heat vertically and this is done twice a day. So we can not expect large variations in the amount of heat induced by short term variations.

d) It is difficult based in what was done here, to have a figure; we can guess 5% of the amount of heat.

Another possible application of the results obtained is the following: Assume the amount of heat for a given day in a given geographical position is $Q(t_1)$ and that $\underline{n}$ days latter is $Q(t_2)$. The sea surface temperature difference between these two days will be

$$T(t_2) - T(t_1) = \frac{1}{\rho c_p} \left[\frac{Q(t_2)}{h(t_2)} - \frac{Q(t_1)}{h(t_1)} \right] \qquad (6.3.1)$$

The expression (6.3.1) can be used to estimate the accuracy of sea surface temperature measured from satellite

Another point that deserves some comments is the fact that since the waves observed are of a non-linear nature, how could the features discussed be reasonably well explained by such a crude model?

Note that (2.1.7) is a first approximation to

$$c = c_0 \left[1 - \frac{1}{6} k^2 \left(\frac{k \rho_2 h_1^2 + 3 \rho_1 h_1}{k \rho_2} \right) + O(k^4 h_1^4) \right]$$

where

$$c_0^2 = g \frac{(\rho_2 - \rho_1)}{\rho_2} h_1$$

and this is a dispersion relation of a non-linear wave as explained in Benjamin (1967).

7. CONCLUSIONS

Landsat A/B images taken in July and August of 1972, 1973 and 1974 were used with a simple two-layer ocean model to compute the mixed layer depth and the amount of heat stored over the continental shelf between Nova Scotia and Cape Hateras.

It was found that a comparison of mixed layer depth computed from satellite and observed from the few in-situ observations is almost impossible due to the internal wave noise introduced in the hydrographic observations. The comparison between the values of the amount of heat stored gives a reasonable agreement. The values of the heat stored from in-situ observation are larger.

During the month of July the mixed layer depth was found deeper than for August. The reason is wind mixing; the winds are stronger in July. The amount of heat in August is less than in July, probably because the larger amount of fog in July acts as a radiative blanket and also as an evaporation shield.

An estimation of the accuracy in determination of the amount of heat Q and the mixed layer depth h, was done resulting in a fractional percentage error of 8% for Q and 32% for h. The effect of the inclusion of the Coriolis parameter in the mixed layer depth computation was found to be negligible.

An extension for a three-layer model was unsuccessful because of the appearance of new variables which we cannot estimate either from satellite of from climatology. The Boussinesq approximation applied to the three-layer model put some constraints on the waves described.

The model can be used to estimate the accuracy of sea surface temperature taken from satellites. As a recommendation for an improvement in the comparisons we suggest a buoy moored at a geographical location chosen on the basis of satellite image.

REFERENCES

Apel, J.R.; Charnell, R.L.; Blackwell, R.J. (1974). Ocean internal waves off the North American and African coasts from ERTS-1. Collected Reprints - 1974, Vol. I, Atlantic Oceanographic and Meteorological Laboratories. U.S. Department of Commerce, NOAA.

Apel, J.R.; Byrne, H.M.; Proni, J.R.; Charnell, R.L. (1975). Observations of oceanic internal and surface waves from the Earth Resources Technology Satellite. J. Geophys. Res., 80 (6), 865-881.

Apel, J.R.; Byrne, H.M.; Proni, J.R.; Sellers, R. (1976). A study of oceanic internal waves using satellite imagery and ship data. Remote Sensing of Environment, 5, 125-135.

Barbee, W.B. (1975). Measurement of internal waves of tidal frequency near a continental boundary. J. Geophys. Res.,80 (15), 1965-1974.

Benjamin, T.B. (1967). Internal waves of permanent form in fluids of great depth. J. Fluid Mech., 29, 559-592.

Bumpus, D.F.; Lautier, L.M. (1965). Surface Circulation on the Continental Shelf off Eastern North America between Newfoundland and Florida. Serial Atlas of the Marine Environment, folio 7, American Geographical Society.

Defant, A. (1961). Physical Oceanography, Vol. 2, Pergamon Press, New York.

Ekman, W.V. (1905). On the influence of the earth's rotation on ocean currents. KGL. Svenska Vetenskapsakao. Arkiv for Mat., Astron., Fysik, 2 (11).

Ewing, G. (1950). Slicks, surface films and internal waves. J. Marine Res. 9, 161-187.

Gargett, A.E. and Hughes, B.A. (1972). On the interaction of surface and internal waves. J. Fluid Mech., 52, 6573-6584.

Halpern, D. (1971). Semidiurnal internal tides in Massachusetts Bay. J. Mar. Res., 29, 116-131.

Ketchum, B.H. and Corwin, N. (1974). The persistence of winter water on the continental shelf south of Long Island, New York. Limn. Oceanogr., 9, 467-475.

Laevastu, T. (1963). Factors affecting the temperature of the surface layer of the sea. Soc. Sci. Fennica. Commentationes Phys. Math. 25 (1).

La Fond, E.C. (1959). Sea-surface features and internal waves in the sea. Indian J. Meteorol. Geophys., 10, 415-419.

Lamb, H. (1932). Hydrodynamics. Dover Publications, New York.

Langmuir, I. (1938). Surface motion of water induced by wind. Science, 87 (2250), 119-123.

Munk, W.H. and Anderson, E.R. (1948). Notes on a theory of the thermocline. J. Marine Res., 7 (3), 276-295.

Phillips, O.M. (1977). The Dynamics of the Upper Ocean. Cambridge University Press, London.

Rattray, M. (1960). On coastal generation of internal tides. Tellus, 12 (1), 54-62.

Roberts, J. (1975). Internal gravity waves in the ocean. Marine Science, Volume 2, Marcel Dekker, Inc., New York.

Rossby, C.G. and Montgomery, R.B. (1935). The layer of frictional influence in wind and ocean currents. Papers Phys. Oceanog. Meteorol. Mass Inst. Technol. and Woods Hole Oceanog. Inst., 3 (1).

Sawyer, C. and Apel, J.R. (1976). Satellite images of ocean internal-wave signatures. Environmental Research Laboratories, NOAA S/T 2401.

Shand, J.A. (1953). Internal waves in Georgia Strait. Trans. Amer. Geophys. Un., 34, 849-856.

Stommel, H; Von Arx, W.S.; Parson, D.; Richardson, W.S. (1953). Rapid aerial survey of Gulf Stream with camera and radiation thermometer. Science, 117 (3049), 639-640.

Tabata, S; Boston, N.E.; Boyce, F.M. (1965). The relation between wind speed and summer isothermal surface layer of water at Ocean Station P in the Eastern Subarctic Pacific Ocean. J. Geophys. Res. 70 (16), 3867-3878.

Thompson, A.J. and West, B.J. (1972). Interaction of non-saturated surface gravity waves with internal waves. Tech. Rep. RADC-TR-72-280. Phys. Dyn. Inc., Berkeley, Calif. (ARPA order 1649).

Thorpe, S.A. (1968). On the shape of progressive internal waves. Proc. Roy. Soc. A 1145, 263, 563-613.

Turner, J.S. (1973). Buoyancy Effects in Fluids. Cambridge University Press, London.

U.S. Department of the Navy, Hydrographic Office (1959). Climatological and Oceanographic Atlas for Mariners. Volume 5, North Atlantic Ocean.

Veronis, G. (1973). Large scale circulation. Advances in Applied Mechanics, Vol. 13, Academic Press, Inc., New York and London.

Williams, R.G.; Godshall, F.A. (1977). Summerization and Interpretation of Historical Physical Oceanographic and Meteorological Information for the Mid-Atlantic Region. Final Report, AA550-IAG-12. U.S. Department of Commerce, NOAA.